Characterization of age-associated immunity in atherosclerosis

Smit, V.

Chapter 3

Single-cell profiling reveals age-associated immunity in atherosclerosis

Virginia Smit[1], Jill de Mol[1], Frank H. Schaftenaar[1], Marie A.C. Depuydt[1], Rimke J. Postel[1], Diede Smeets[1], Fenne W.M. Verheijen[1], Laurens Bogers[1], Janine van Duijn[1], Robin A.F. Verwilligen[1], Hendrika W. Grievink[1,2], Mireia N.A. Bernabé Kleijn[1], Eva van Ingen[1], Maaike J.M. de Jong[1], Lauren Goncalves[3], Judith A.H.M. Peeters[3], Harm J. Smeets[3], Anouk Wezel[3], Julia K. Polansky[4], Menno P.J. de Winther[5], Christoph J. Binder[6], Dimitrios Tsiantoulas[6], Ilze Bot[1], Johan Kuiper[1], and Amanda C. Foks[1]

[1] Leiden Academic Centre for Drug Research, Division of BioTherapeutics, Leiden University, Einsteinweg 55, 2333 CC Leiden, The Netherlands.
[2] Centre for Human Drug Research, Zernikedreef 8, 2333 CL Leiden, The Netherlands.
[3] Department of Surgery, Haaglanden Medical Center – location Westeinde, Lijnbaan 32 2515 VA The Hague, The Netherlands.
[4] Berlin Institute of Health at Charité – Universitätsmedizin Berlin, BIH Center for Regenerative Therapies (BCRT), Charitéplatz 1, 10117 Berlin, Germany.
[5] Amsterdam University Medical Centers – location AMC, University of Amsterdam, Experimental Vascular Biology, Department of Medical Biochemistry, Amsterdam Cardiovascular Sciences, Meibergdreef 9, 1105 AZ Amsterdam, The Netherlands.
[6] Department of Laboratory Medicine, Medical University of Vienna, Lazarettgasse 14, AKH BT25.2, 1090 Vienna, Austria.

Published in Cardiovascular Research, 2023 Jun 30, doi: 10.1093/cvr/cvad099

ABSTRACT

Aims

Aging is a dominant driver of atherosclerosis and induces a series of immunological alterations, called immunosenescence. Given the demographic shift towards elderly, elucidating the unknown impact of aging on the immunological landscape in atherosclerosis is highly relevant. While the young Western diet-fed *Ldlr*-deficient (*Ldlr*$^{-/-}$) mouse is a widely used model to study atherosclerosis, it does not reflect the gradual plaque progression in the context of an aging immune system as occurs in humans.

Methods and results

Here, we show that aging promotes advanced atherosclerosis in chow diet-fed *Ldlr*$^{-/-}$ mice, with increased incidence of calcification and cholesterol crystals. We observed systemic immunosenescence, including myeloid skewing and T-cells with more extreme effector phenotypes. Using a combination of single-cell RNA-sequencing and flow cytometry on aortic leukocytes of young versus aged *Ldlr*$^{-/-}$ mice, we show age-related shifts in expression of genes involved in atherogenic processes, such as cellular activation and cytokine production. We identified age-associated cells with pro-inflammatory features, including GzmK^{+}CD8^{+} T-cells and previously in atherosclerosis undefined CD11b^{+}CD11c^{+}T-bet^{+} age-associated B-cells (ABCs). ABCs of *Ldlr*$^{-/-}$ mice showed high expression of genes involved in plasma cell differentiation, co-stimulation, and antigen presentation. *In vitro* studies supported that ABCs are highly potent antigen-presenting cells. In cardiovascular disease patients, we confirmed the presence of these age-associated T- and B-cells in atherosclerotic plaques and blood.

Conclusions

Collectively, we are the first to provide comprehensive profiling of aged immunity in atherosclerotic mice and reveal the emergence of age-associated T- and B-cells in the atherosclerotic aorta. Further research into age-associated immunity may contribute to novel diagnostic and therapeutic tools to combat cardiovascular disease.

Keywords: cardiovascular disease, atherosclerosis, aging, immunology, immunosenescence

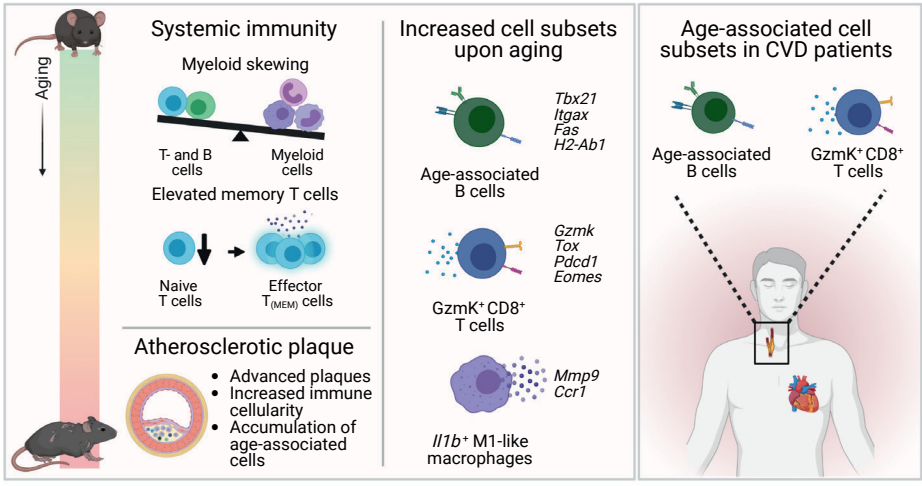

Graphical Abstract

INTRODUCTION

Aging is a complex process that gradually affects multiple physiological systems in the body. During aging, cell-intrinsic and microenvironmental changes of the bone marrow cause hematopoietic stem cells (HSCs) and progenitors to deviate from lymphopoiesis and preferentially differentiate towards myeloid lineages, resulting in expansion of the myeloid cell pool. Concurrently, age-induced structural changes of lymphoid organs cause a strong reduction in peripheral lymphocytes.[1,2] Together with a gradual functional decline of immune cells, these age-related changes of the immune system are termed "immunosenescence".[3] Immunosenescence can promote a chronic state of low-grade inflammation called "inflammaging".[4] As a result, the elderly are more susceptible to infections, autoimmune diseases and chronic vascular diseases such as atherosclerosis, which is the main underlying cause of cardiovascular disease (CVD).[3,5] Aging is actually one of the main risk factors for CVD, as the prevalence and consequent mortality associated with CVD increase with age. In 2019, CVD accounted for more than one-third (3.4 million) of total deaths in the global population aged 60-69 and up to nearly half (11.5 million) of total deaths in age groups of 70 years and older.[6] Together with a large demographic shift towards an older population, it has become a major public health priority to improve our understanding of age-associated maladaptive immunity as a cause of disease susceptibility and mortality.

Both myeloid and lymphoid cells contribute to the formation of atherosclerotic plaques in the arterial wall[7] and transcriptome analyses of aortic leukocytes in murine models of atherosclerosis have revealed high diversity amongst immune cells in the plaque.[8,9] The vast majority of experimental studies investigating immunity and immune modulating therapies in atherosclerosis has been performed in relatively young animals fed a Western diet (3-6 months of age, resembling adolescents aged 20-30 years), whereas CVD patients receiving treatment are often of advanced age (~60 years at first coronary artery disease diagnosis)[10] and have an aged immune system, which limits the translation of experimental findings to the patient. In addition, accelerated development of Western diet-induced atherosclerosis in young mice does not resemble the gradual process of plaque development and progression in humans. It is therefore of utmost importance to take aging into consideration in experimental atherosclerosis studies. To obtain in-depth insight in the atherosclerotic immune responses that arise upon aging, we profiled age-associated systemic immunity by a high throughput analysis and investigated atherosclerotic lesion development in young (5 months) and aged (22 months, correlating with humans of ~60 years of age) low-density lipoprotein receptor-deficient (*Ldlr*$^{-/-}$) mice. Using single-cell RNA-sequencing (scRNA-seq) we compared the transcriptomic profile of aortic leukocytes from chow diet- and Western diet-fed young *Ldlr*$^{-/-}$ mice to chow diet-fed aged atherosclerotic *Ldlr*$^{-/-}$ mice and revealed age-associated immune cell subsets, including age-associated GzmK^{+}CD8^{+} T-cells and age-associated B-cells, in atherosclerotic mice and cardiovascular disease patients.

METHODS

A detailed version of the Methods is available in the Supplementary material.

Animals

All animal experiments were approved by the Leiden University Animal Ethics Committee and were performed according to the guidelines of the European Parliament Directive 2010/63/EU of the European Parliament. Female C57BL/6J, *Ldlr*$^{-/-}$ and *Apoe*$^{-/-}$ mice (if not specified elsewhere: young, 3 months or aged, 20 months old), and OTII mice (4 months old) on a C57Bl/6J genetic background were bred and aged in-house and kept under standard laboratory conditions. C57BL/6J, and *Apoe*$^{-/-}$ and OTII mice were fed a regular chow diet (CD). Aged *Ldlr*$^{-/-}$ mice were fed a CD, while young mice were fed a CD or a Western diet (WD) containing 0.25% cholesterol and 15% cocoa butter (Special Diet Services, Witham, Essex, UK) for 10 weeks. At the end of experiment, mice were terminally anaesthetized by a subcutaneous injection of a cocktail contain ketamine (100 mg/kg), atropine (50 µg/mL), and xylazine (10 mg/kg). Mice were bled by retro-orbital bleeding and tissues were harvested after *in situ* perfusion with PBS.

Patient population

Human atherosclerotic plaques (n=9-15) and paired blood samples were obtained from patients undergoing a carotid endarterectomy procedure at the Haaglanden Medical Center, location Westeinde (The Hague, The Netherlands). The study was approved by the Medical Ethical Committee of the HMC (NL71516.058.19). The study was performed in accordance with the declaration of Helsinki and all patients gave written informed consent at the start of the study.

Serum cholesterol, triglyceride and immunoglobulin measurements

To determine total cholesterol and triglyceride levels, mouse serum samples underwent enzymatic colorimetric procedures (Roche/Hitachi, Mannheim Germany) with precipath (Roche/Hitachi) as an internal standard. Total serum titers of IgM and oxLDL-specific IgM were measured by ELISA as previously described.[11]

Histology

Hearts and aortas were embedded in O.C.T. compound (Sakura) and snap-frozen. To determine lesion size, cryosections (10 µm) of the aortic root were stained with Oil-Red-O and hematoxylin (Sigma-Aldrich). Collagen content was quantified using a Masson's trichrome staining (Sigma-Aldrich). The necrotic core was defined as the acellular, debris-rich lesion area as percentage of total plaque area. Corresponding sections on separate slides were stained for monocyte/macrophage content with a MOMA-2 antibody (1:1000, AbD Serotec) followed by secondary antibody. We categorized cholesterol crystallization of atherosclerotic lesions in the

aortic root on a scale of 0 (no cholesterol crystallization) to 3 (>75% of the lesion area contains crystalline cholesterol). Presence of calcification was manually scored based on morphology. Analysis and scoring were performed blinded. Mice with bicuspid aortic valves were excluded from histological analyses (n=3). Pictures were taken with a Mikrocam II (Besser) linked to a Leica DM6000 Microscope. Stained sections were manually analysed with ImageJ software.

Human tissue processing

Single cell suspensions of human carotid plaques were obtained as previously described.[12]

Flow cytometry

Immunostaining was performed as previously described [13] on single cell suspensions derived from murine blood, spleen, and aortas, and human PBMCs and plaques to characterize immune cells. Living cells were selected using Fixable Viability Dye eFluor™ 780 (1:2000, eBioscience) and different cell populations were defined using anti-mouse and anti-human fluorochrome-conjugated antibodies (Major Resources Table in the Supplementary material). Antibody staining of transcription factors and cytokines was performed using transcription factor fixation/permeabilization concentrate and diluent solutions and cytofix/permeabilization solutions, respectively (BD Biosciences). FACS analysis was performed on a Cytoflex S (Beckman Coulter) and the acquired data were analyzed using FlowJo software.

Aortic CD45$^+$ cell isolation for single-cell RNA-sequencing

Atherosclerotic aortic arches, from which perivascular adipose tissue was removed, were isolated from young WD-fed (young WD) *Ldlr*$^{-/-}$ mice (4-5 months old; n=29) and old CD-fed (old CD) *Ldlr*$^{-/-}$ mice (22 months old; n=12) and enzymatically digested. Single cell suspensions were stained with Fixable Viability Dye eFluor™ 780 (1:2000, eBioscience) and CD45-PE (1:500, clone 30-F11, Biolegend). After removing doublets, alive CD45$^+$ cells were sorted (Supplementary material Figure S1a) using a FACS Aria II SORP (BD Biosciences) and loaded on a Chromium Single Cell instrument (10x Genomics) to prepare single-cell RNA-sequencing (scRNA-seq) libraries. Sequencing was performed on an Illumina HiSeq2500 and the digital expression matrix was generated by de-multiplexing barcode processing and gene UMI (unique molecular index) counting using the Cell Ranger v3.0 (aged) and v6.0 (young) pipeline (10x Genomics). Data quality is provided in Supplementary material Figure S1b-d.

Single-cell data processing and integrative analysis

Digital expression matrices were analyzed using the Seurat package in R. Low quality cells were excluded by setting thresholds for unique gene count reads and mitochondrial gene expression (Supplementary material Figure S1c). Using the DoubletDecon approach[14], doublets were removed. Single-cell transcriptomes of CD45$^+$ cells isolated from aortas of young non-

atherosclerotic chow diet-fed *Ldlr*$^{-/-}$ mice (2 months old, n=9; GSM2882368)[9] were loaded and filtered from doublets and low-quality cells.

Next, transcriptomes of the three datasets were integrated to perform comparative analysis on the remaining 372 (young CD), 4319 (young WD) and 4674 (old CD) cell counts, followed by clustering. For the high-resolution re-clustering, (*Cd79b*$^{+}$) B-cell clusters, (*Cd3e*$^{+}$) T-cell clusters and (*Cd68*$^{+}$ and *Itgam*$^{+}$) myeloid clusters were selected and extracted from the main clustering. Reclustering on rescaled transcripts was performed resulting in: T-cells (3561 cells), B-cells (2269 cells), and myeloid cells (1166 cells). Within cluster 2 of the B-cell clustering, bonafide age-associated B-cells (ABCs) were separated from plasma cells (PCs) by setting a threshold on *Igkc* expression levels: ABCs, *Igkc*<6.3 and PCs, *Igkc*>6.3 (Supplementary material Figure S6h). Differential gene expression of bonafide ABCs was used for volcano plot generation and pathway analysis in Figure 4. Pathway analysis was performed using Ingenuine Pathway Analysis (IPA) Software (Qiagen).

Projection of scRNA-seq analysis of aortic cells of non-atherosclerotic C57BL/6 mice onto *Ldlr*$^{-/-}$ aortas

ScRNA-seq data of C57BL/6 mice of 3-24 months of age[15], were loaded and excluded of non-immune cells (e.g. endothelial cells; Supplementary material Figure S6b). A total of 45 (3 months), 27 (18 months), and 19 (24 months) aortic immune cells were included in this analysis and set as query dataset. Our scRNA-seq dataset of atherosclerotic aortas from *Ldlr*$^{-/-}$ mice was set as reference dataset. With the MapQuery function, the query cells were projected onto the *Ldlr*$^{-/-}$ UMAP structure.

PMA/ionomycin stimulation

Single cell suspensions from spleen were stimulated for 4 hours with PMA (50 ng/ml, Sigma), ionomycin (500 ng/ml, Sigma) and the Golgi-plug brefeldin A (3 μg/ml, Thermofisher) to detect intracellular cytokine expression with flow cytometry.

In vitro antigen presentation assay

Splenic ABCs and follicular (FO) B-cells were isolated from aged female *Ldlr*$^{-/-}$ mice (aged 12-20 months old, n=5) and exposed to OVA323 peptide antigen or control medium for 4 hours at 37ºC 5% CO2. Next, B-cells were co-cultured in a 1:1 ratio with CD4^{+} T-cells from OTII mice for 24 hours, after which activated CD69^{+} cells were measured as percentage CD4^{+} T-cells with flow cytometry. Proliferation was assessed by co-culturing OVA323-exposed B-cells with CFSE-labeled CD4^{+} T-cells for 72 hours, followed by measurement of CFSE dilution.

Macrophage polarization and in vitro phagocytosis assay

M1 and M2 bone marrow-derived macrophages (BMDMs) from young and aged chow diet-fed *Ldlr*$^{-/-}$ mice (n=5 per group). To assess efferocytosis capacity, M1 and M2 macrophages were exposed to CFSE-labeled apoptotic splenocytes for 2h, after which uptake was measured by flow cytometry. To assess lipid uptake, macrophages were cultured with 4 μM cholesteryl-BODIPY FL C_{12} (Invitrogen, #C3927MP) for 24h, followed by measurement of alive BODIPY^{+} (lipid-laden) macrophages using flow cytometry.

Statistical analysis

Data are expressed as mean ± SEM. Outliers were identified and removed using Grubbs outlier tests (α = 0.05). Significance of mouse data with 3 groups was tested using an ordinary one-way ANOVA test or nonparametric Kruskal-Wallis test followed by a Tukey or Dunn multiple comparisons test, respectively. Significance of young versus aged BMDMs was tested by two-tailed unpaired t-test. Significance of follicular B-cells versus age-associated B-cells was tested by two-tailed paired t-test. Significance of human data was tested using a two-tailed paired t-test. P-values of <0.05 were considered significant. Statistical analysis was performed using GraphPad Prism 9.0.

Data availability

In silico data analysis was performed using custom R scripts (R version 4.1.2) designed especially for this research and/or based on the recommended pipelines from the pre-existing packages listed in the individual segments above. Single-cell RNA sequencing data are available upon personal request from the corresponding author (a.c.foks@lacdr.leidenuniv.nl).

RESULTS

Myeloid skewing and reduced lymphoid output in aged *Ldlr*$^{-/-}$ mice

We set out to investigate the impact of aging on innate and adaptive immunity in atherosclerosis. To this extent, leukocyte populations were characterized in the circulation and lymphoid organs of chow diet-fed (CD) or Western diet-fed (WD) young (5 months) and old CD (22 months) *Ldlr*$^{-/-}$ mice (Figure 1a). Circulating myeloid CD11b^{+} cells, including neutrophils and inflammatory monocytes, were elevated with age (Figure 1b). Conversely, the lymphoid output, as measured by CD4^{+} and CD8^{+} T-cells and CD19^{+} B-cells in the blood, was decreased upon aging (Figure 1c-f). Within the T-cell compartment, aging significantly reduced the proportion of circulating naïve CD8^{+} T-cells, whereas central memory CD4^{+} and CD8^{+} T-cells were increased (Supplementary material Figure S2a). More apparent shifts from naïve to memory T-cell populations were observed in the spleen (Figure 1d). Besides changes in lymphoid output, aging can also affect the activation status of lymphocytes.[3] As shown in

Figure 1e, T-cells producing interferon-γ (IFN-γ), interleukin-4 (IL-4), IL-10 and IL-17 were elevated in aged *Ldlr*$^{-/-}$ mice, indicating enhanced regulatory and effector T-cell functionality. Since aging can also alter humoral immunity[16], we measured antibody levels in the serum. Total serum immunoglobulin G1 (IgG1) and IgG2c levels remained unchanged in aged mice compared to young mice (data not shown), while total IgM and oxidized LDL-specific IgM (oxLDL-IgM) levels were increased upon aging (Figure 1g).

Single-cell transcriptomic profile shows age-associated immune alterations in atherosclerotic *Ldlr*$^{-/-}$ aortas

We next mapped the immunological landscape of the aged atherosclerotic plaque by performing scRNA-seq (10x Genomics Chromium) on fluorescence-activated cell sorted (FACS) CD45^{+} cells from the aortic arch of aged atherosclerotic *Ldlr*$^{-/-}$ mice (old CD, Figure 2a). To define age-associated changes in aortic leukocytes, we integrated scRNA-seq data of aortic CD45^{+} cells from non-atherosclerotic young CD *Ldlr*$^{-/-}$ mice[9] and atherosclerotic young WD *Ldlr*$^{-/-}$ mice, which currently is one of the most frequently used atherosclerosis models.

Analysis of 372 (young CD), 4319 (young WD), and 4674 (old CD) single-cell transcriptomes with a Uniform Manifold Approximation and Projection (UMAP) projection revealed 16 distinct immune cell clusters in the atherosclerotic aorta (Figure 2b-c and Supplementary material Figure S3a-b), providing, to our knowledge, the first comprehensive atlas of immune cells present in atherosclerotic aortas of aged *Ldlr*$^{-/-}$ mice. We assigned biological identities to major immune cells by interrogating expression patterns and canonical marker genes[17] (Supplementary material Figure S3c-d and Table S1): B-cells (*Cd79a, Cd19*), T-cells (*Cd3e, Cd4, Cd8a, Tcrg-c1*), natural killer (NK) cells (*Klr1bc, Ncr1*), and myeloid cell populations (*Itgam, Cd68, Adgre1*). Among CD45^{+} cells in the aorta of young CD, WD and old CD mice, myeloid cell clusters (cl. 4, 6, 8, 11, 12, 15) accounted for 22% in young CD, 12% in young WD and 27% in old CD mice, *Cd79a*$^{+}$ B-cells (cl. 1, 7) for 23% in young CD, 22% in young WD and 29% in old CD mice, and *Klrb1c*$^{+}$ NK cells (cl. 14) for 2% in young CD and 1% in both young WD and old CD mice, while *Cd3e*$^{+}$ T-cells (cl. 0, 2, 3, 5, 9, 10, 13) were the most abundant (53% in young CD, 65% in young WD and 42% in aged CD mice; Figure 2d).

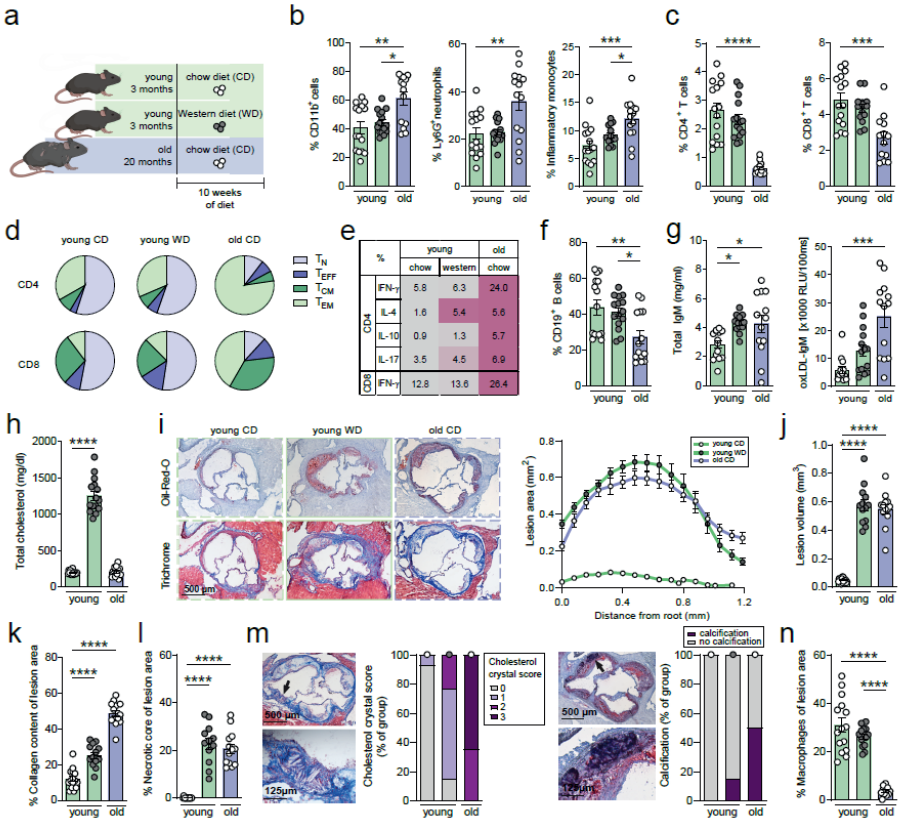

Figure 1. Aging promotes immunosenescence and atherosclerosis in *Ldlr*$^{-/-}$ mice.

a, Experimental setup: *Ldlr*$^{-/-}$ mice aged 3 months (green bars) or 20 months (violet bars) were fed a standard chow diet (white circles) or a Western diet (grey circles) for 10 weeks. **b**, Using flow cytometry, percentages (% from live) of circulating myeloid cells (CD11b^{+}), neutrophils (CD11b^{+}Ly6C^{int}Ly6G^{+}), inflammatory monocytes (CD11b^{+}Ly6C^{hi}Ly6G^{-}), **c**, circulating CD4^{+} and CD8^{+} T-cells were determined (% from live). **d**, Splenic naïve (T_N: CD44^{-}CD62L^{+}), effector (T_{EFF}: CD44^{-}CD62L^{-}), central memory (T_{CM}: CD44^{+}CD62L^{+}) and effector memory (T_{EM}: CD44^{+}CD62L^{-}) T-cells were quantified as a percentage of CD4^{+} and CD8^{+} T-cells and plotted in pie charts. **e**, Intracellular cytokine production of interferon-gamma (IFN-γ), interleukin (IL)-4, IL-10 and IL-17 were measured as percentage (mean) of splenic CD4^{+} and CD8^{+} T-cells after 4 hours of stimulation with PMA and ionomycin. Color scale is normalized for each cytokine. **f**, Circulating CD19^{+} B-cells were determined with flow cytometry. **g**, Total and oxidized LDL(oxLDL)-specific IgM titers were measured in the serum. **h**, Total serum cholesterol levels at sacrifice were measured. **i**, Cross sections of the aortic root were stained for lipid and collagen content and **j**, atherosclerotic lesion volume was quantified. **k**, Collagen content and **l**, necrotic cores were quantified as percentage of lesion area. **m**, Cholesterol crystallization in atherosclerotic lesions was categorized on a scale of 0 (no cholesterol crystallization) to 3, and presence of calcification (purple) or no calcification (grey) was presented as percentage of group. **n**, Macrophage content (MOMA-2) was measured as percentage of lesion area. Data are from n=12–15 mice per group. Statistical significance was tested by one-way ANOVA. Mean ± SEM plotted. *P<0.05, **P<0.01, ***P<0.001, ****P<0.0001.

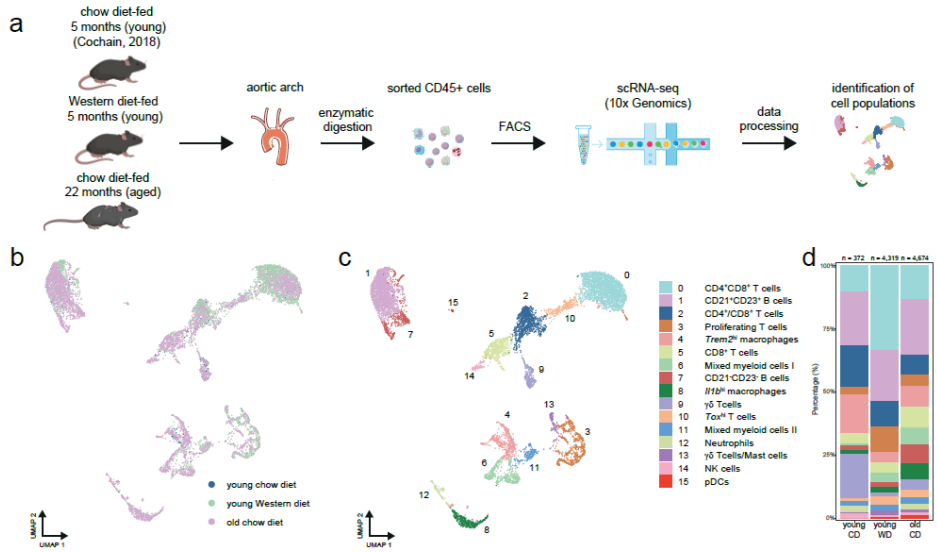

Figure 2. Integrated scRNA-seq analysis reveals age-associated leukocyte alterations in atherosclerotic mouse aortas.
a, Workflow of scRNA-seq on aortic CD45$^+$ cells of chow diet-fed young *Ldlr*$^{-/-}$ mice (young CD, n=9)[9], or Western diet-fed (10 weeks) young *Ldlr*$^{-/-}$ mice (young WD, n=29) and chow diet-fed aged *Ldlr*$^{-/-}$ mice (old CD, n=12). UMAP visualization of clustered aortic leukocytes grouped by **b**, sample or **c**, immune cell clusters. **d**, Stacked diagram showing the relative proportions of major immune cell subtypes within CD45$^+$ cells of *Ldlr*$^{-/-}$ aortas. NK: natural killer, pDC: plasmacytoid dendritic cell.

Integrated scRNA-seq analysis of T-cells reveals a large CD8$^+$GzmK$^+$T cell population in aged atherosclerotic aortas

Although T-cells have been well-described in atherosclerosis progression, in the lymphoid system and locally in the lesion[18], the impact of aging on T-cell subsets remains largely unknown. To identify age-associated alterations within the T-cell compartment in atherosclerotic aortas, we reclustered the *Cd3e*$^+$ T-cells from the principal clustering, resulting in 12 distinct clusters (Figure 3a-b and Supplementary material Figure S4a).

Three T-cell clusters (cl. 0, 1 and 4) co-expressed *Cd4* and *Cd8* (Figure 3c). Cluster 0 and 1 exhibited a gene expression profile similar to that of late stage CD4$^+$CD8$^+$ double positive (DP) thymocytes.[19,20] Besides high expression level of *Rorc*, leading differentially expressed genes (DEGs) of cluster 1 and 2 included *Rag1* and *Ccr9* (Figure 3d & Table S2). Comparative analysis between cluster 0 and 1 showed higher expression of *Ifngr1*, *Ly6d*, *Lgals1* and *Anxa2*, while *Malat1*, *Rag1* and *Glcc1* were less expressed in cluster 0 compared to cluster 1 Supplementary material Figure S4b). Cluster 4 (DP T-cells) and 6 (*Cd4*$^-$*Cd8*$^+$ T-cells) were enriched in genes associated with cell organization and cell cycle processes (*Nusap1*, *Top2a* and *Mki67*), suggesting that these clusters are distinguished by their (proliferative) cell cycle state (Table S2). Specifically, some DP cells and proliferating *Cd8*$^+$ T-cells (cluster 1, 4 and 6) expressed *Gzma*, indicating cytotoxic properties (Figure 3c and Supplementary material

Figure S4c). Adjacent to the large $CD4^+CD8^+$ population, cluster 3 is located, which contains *Tox*^{hi} $CD4^+CD8^+$ DP, $CD4^+$ and $CD8^+$ single positive (SP) T-cells (Figure 3b). Top DEGs in this cluster were *Itm2a*, *Tox* and *Lef1*, which are usually involved in DP thymocyte selection, activation and differentiation.[21,22]

Cluster 2 contains $CD4^+$ and $CD8^+$ SP T-cells, and is defined by T-cell activation state, as we observed a gradient of *Cd44* and *Sell* (CD62L) expression, indicating the presence of naïve or quiescent T-cells, and memory T-cells. While *Cd44*$^-$ *Sell*$^+$ naïve-like cells were mainly found in the aorta of young CD and WD mice, *Cd44*$^+$ cells were mostly present in the aged atherosclerotic aorta (Supplementary material Figure S4d). Although we could not retrieve distinct clusters of typical $CD4^+$ T-cell subsets (e.g. Th1 or Th2 cells), we identified a $CD4^+$ T-cell cluster (cluster 8) that mainly contained regulatory T-cells (Tregs) expressing *Foxp3*, *Izumo1r* (folate receptor 4), *Tnfrsf4* (OX40), *Ctla4* and *Nt5e*.[23] Tregs from aged *Ldlr*$^{-/-}$ mice showed higher expression of *Ctla4, Lag3*, and *Tnfrsf4*, in addition to higher expression of cytokines (e.g. *Tgfb1* and *Ebi3* that encodes for the IL-35 subunit; Figure 3g).

Cluster 5 contained $CD8^+$ T-cells with a gene expression profile suggestive of an effector (*Nkg7*, *Gzmk*, *Gzmb*, *Fasl*), but also exhausted (*Eomes*, *Pdcd1, Lag3*) phenotype. The signature of these cells (Figure 3g and Supplementary material Figure S4e) resemble the recently described age-associated granzyme K (*Gzmk*)-expressing $CD8^+$ T (Taa) cells.[24] Indeed, these Taa cells were almost absent in young CD aortas, and mostly present in the aorta of old CD mice (Figure 3b). Compared to other $CD8^+$-T cells in cluster 2, 3 and 6, Taa cells highly expressed *Gzmk*, *Ccl5*, *Nkg7*, *Cd52*, and *Id2*, indicating again an effector and memory phenotype (Figure 3e and S4f). Th1/Th2 and NK signaling pathways were enriched in cluster 5 (Figure 3f), suggesting that these cells might be active effector cells.[25] When we compare the few *Gzmk*$^+$ $CD8^+$ T-cells found in young aortas with the *Gzmk*$^+$ $CD8^+$ T-cells found in old CD aortas, aged *Gzmk*$^+$ $CD8^+$ T-cells showed high expression of exhaustion-associated markers and effector molecules *Gzmk*, and *Prf1*, indicating a more extreme phenotype in aged than in young atherosclerotic aortas (Figure 3g).

Enrichment of NK-marker genes (*Klre1, Klrk1, Klrb1c*) and cytotoxic marker genes *Gzmb* and *Gzmm* were observed in cluster 9, indicative of NKT-cells. Besides conventional αβ T-cells, we also identified γδ T-cells in clusters 7 and 11. Cluster 11 is most likely a mix of γδ T-cells and progenitor-like mast cells (*Nfe2*, *Cd34*, *Cpa3* and *Gata2;* Figure 3c, Table S2), whereas cluster 7 exclusively expressed *Il17a* (Figure 3c and 3g), consistent with IL-17-producing γδT17 cells.[26] We detected few remainder *Cd3e*$^-$ mast cells (*Kit*, *Gata2*, *Fcer1a*) in cluster 10.

Overall, T-cells in aortas from young mice mainly include naïve, developing and proliferating T-cells, while T-cells from old atherosclerotic aortas exhibit increased expression of activation

markers (e.g. *Crtam*, *Adgre5*; Figure 3g) and mostly consist of effector (memory) T-cells, Tregs and age-associated T-cells.

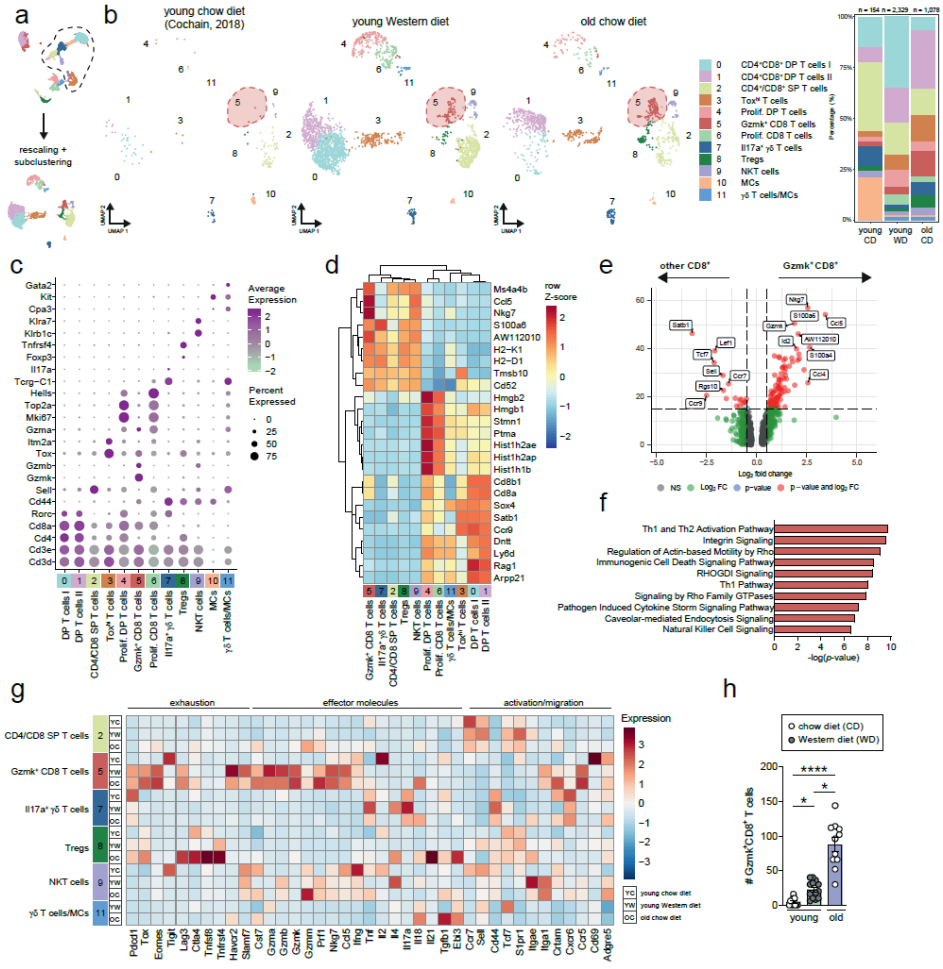

Figure 3. Identification of age-associated T-cell populations and gene signatures in atherosclerotic aortas from *Ldlr*$^{-/-}$ mice.
a, *Cd3e*$^{+}$ clusters were extracted from the principal clustering and reclustered, after which the T-cell clusters were identified. **b**, UMAP plots and stacked diagrams visualizing the identified T-cell subclusters in young CD, young WD and old CD aortas, in which Gzmk^{+}CD8^{+} T-cells are encircled in the dashed red shape. **c**, Dot plot showing the average expression of immune cell cluster-defining markers for each cluster. **d**, Heatmap of hierarchically clustered top 25 variable genes across T-cell subclusters. **e**, Volcano plot of the differentially expressed genes (DEGs) in the Gzmk^{+}CD8^{+} T-cell cluster compared to other CD8^{+} T-cells in cluster 2, 3, 5 and 6. **f**, Top canonical pathways of the Gzmk^{+}CD8^{+} T-cell cluster compared to CD8^{+} T-cells in cluster 2, 3, 5 and 6. **g**, Heatmap showing average expression of biological process-associated genes in T-cell clusters of young CD, young WD and old CD *Ldlr*$^{-/-}$ aortas. **h**, Using flow cytometry, absolute numbers of Ly6C^{-}CD44^{+}Tox^{+}PD-1^{+} CD8^{+} T-cells (GzmK^{+} CD8^{+} T-cells) were measured in aortas of young and aged *Ldlr*$^{-/-}$ mice (n=11-15). Gating strategy is shown in Supplementary material Figure S5b. Statistical significance was tested by one-way ANOVA. Mean ± SEM plotted. *P<0.05, ****P<0.0001. DP: double positive, SP: single positive, Tregs: regulatory T cells, NKT: natural killer T, MC: mast cells.

To validate our age-induced changes found with scRNA-seq, we performed flow cytometry on immune cells within the atherosclerotic aortic arch. $CD4^+$ T-cells, $CD8^+$ T-cells and $CD4^+CD8^+$ DP T-cells within the *Ldlr*$^{-/-}$ aorta were increased upon aging (Supplementary material Figure S4g and S5a). Although present in small numbers in atherosclerotic aortas of young WD mice, we confirmed a significant ~4-fold increase in $Ly6C^-CD44^+Tox^+PD\text{-}1^+$ $CD8^+$ T-cells within the aortas of old CD mice $P<0.05$; Figure 3h and Supplementary material Figure S5b), representing the $Gzmk^+CD8^+$ T-cells.

Identification of age-associated B-cells with pro-inflammatory features in aged atherosclerotic aortas

B-cells in atherosclerosis can be considered pro-atherogenic (B2-cells) or anti-atherogenic (MZ B-cells, B1-cells and regulatory B-cells)[27], and have been found in transcriptomic studies of young atherosclerotic aortas.[8,9] To identify age-associated differences in B-cell subpopulations in the aorta, we reclustered *Cd79a*$^+$ B-cells from the principal clustering at higher resolution (Figure 4a), resulting in the identification of 7 separate cell populations (Figure 4b and Supplementary material Figure S6a). Cells within clusters 0 and 3 show high differential gene expression levels of *Cr2* (CD21), *Fcer2a* (CD23), and *Ighd* (encoding for IgD), which are markers characteristic of mature B2-cells (Figure 4c-d). Cluster 3 contains activated B-cells as they are enriched for genes associated with B-cell activation (*Myc, Egr3, Irf4, Cd83*) and heat-shock protein-associated genes (Figure 4d).[28] Cluster 5 exhibited high expression levels of genes related to the interferon-induced response module (*Ifit3*, *Ifi206*, *Irf7*; Table S3).

Interestingly, *Cr2*^{low} (encoding CD21) clusters 1 and 2 were almost exclusively present in the aorta of old CD mice, but nearly absent in the aortas of young CD mice. Cells within cluster 1 are enriched for markers characteristic of B1-cells as we observed high expression of *Cd9*, *Spn* (CD43), and *Ighm* (IgM), but low expression of *Fcer2a* and *Ighd*. Besides a B1-cell-associated marker, *Cd9* also identifies regulatory B-cells (Bregs).[29] Indeed high levels of Breg-associated genes, including the anti-inflammatory cytokine *Il10, Ebi3, Atf3* and *Slamf9* were detected in cluster 1 (Table S3).[30,31] Interestingly, Bregs of aged mice showed a relative high expression of IL-35-associated *Ebi3*, while young Bregs showed elevated *Il10* expression (Figure 4g), indicating a shift in phenotype upon aging. Moreover, cluster 1 showed high expression of *Zbtb32* (Table S3), a gene involved in plasma cell differentiation, which has previously been observed in splenic and peritoneal CD21^{low} B-cells.[24,32] B-cells within cluster 2 showed co-expression of *Itgam* (CD11b), *Itgax* (CD11c), *Tbx21* (transcription factor T-bet) and *Fas* (Figure 4b and Supplementary material Figure S6b), which we identified as so-called age-associated B-cells (ABCs). ABCs, characterized by the expression of CD11b, and/or CD11c and T-bet, progressively accumulate with age and during autoimmunity.[33–36] Comparison of bonafide ABCs with other B-cell clusters showed a distinct gene signature with high expression of *Tbx21* (transcription factor T-bet), *Fas*, *Zbtb20* and *Ighg3* (Figure 4e). High expression

of *H2-Ab1* (encoding MHCII) and *Dnm3* (dynamin 3, a GTPase involved in endocytosis) (Figure 4d-e) supports previous reports in which ABCs have been described as efficient antigen-presenting cells.[37,38] Correspondingly, signaling pathways associated with phagosome formation and antigen-presentation were enriched in the ABCs (Figure 4f). In addition, ABCs, as well as B1-cells and Bregs, from aged *Ldlr*$^{-/-}$ mice show high expression of co-stimulatory and inhibitory molecules, such as *Tnfsf4* (OX40L), *Tnfsf18* (GITRL), *Tnfrsf8* (CD30), *Cd80*, *Havcr1* (TIM-1) compared to other B-cell clusters (Figure 4g). In support of these data, we show that ABCs from aged atherosclerotic mice are superior in antigen presentation and T-cell activation compared to FO B-cells, as demonstrated by elevated percentages of CD69^{+} CD4 T-cells and vigorous antigen-specific T-cell proliferation upon OVA323 peptide antigen exposure (Figure 4h-i and Supplementary material Figure S6c-e).

Using flow cytometry, we confirmed the large age-induced increase of total B cells and presence of ABCs in aortas of aged *Ldlr*$^{-/-}$ mice based on the expression of CD11b, CD11c and T-bet (young WTD 27±4 cells vs. aged chow 386±53 cells, P<0.01; Figure 4j and Supplementary material Figure S5a and S6f). Accumulation of ABCs in the aorta is not restricted to *Ldlr*$^{-/-}$ mice, as we also observed an age-dependent expansion of ABCs in atherosclerotic *Apoe*$^{-/-}$ mice and non-atherosclerotic C57BL/6 mice. However, healthy aortas of old C57BL/6 mice show reduced ABC numbers compared to age-matched atherosclerotic *Ldlr*$^{-/-}$ and *Apoe*$^{-/-}$ mice, indicative that the atherosclerotic environment promotes expansion of ABCs (Supplementary material Figure S6g).

Besides ABCs, we observed plasma cells (PCs) within cluster 2 that highly expressed *Igkc* (Ig kappa constant; Supplementary material Figure S6h), indicating that these PCs produce high levels of antibodies. These PCs exhibited a relatively low expression of *Cd19*, but high expression of *Sdc1* (Syndecan-1 or CD138), *Xbp1*, *Tnfrsf17* (BCMA)[39] and were mostly present in the aorta of old CD mice (Figure 4b). In cluster 4, we identified immature B-cells, consistent with high expression levels of the transitional B-cell marker *Cd93*. B-cells in cluster 6 showed high expression of *Klf4/6*, *Junb/d,* and *Fos*, which are involved in the suppression of cell proliferation, but are also features of cellular senescence,[40–42] suggesting that these may be senescent B-cells (Figure 4d and Table S3).

Altogether, the B-cell compartment in the atherosclerotic aorta is greatly affected by aging, emphasized by enhanced activation, e.g. elevated expression of co-stimulatory/inhibitory molecules, cytokines, and chemokines, particularly in the B1/Breg and ABC clusters (Figure 4g).

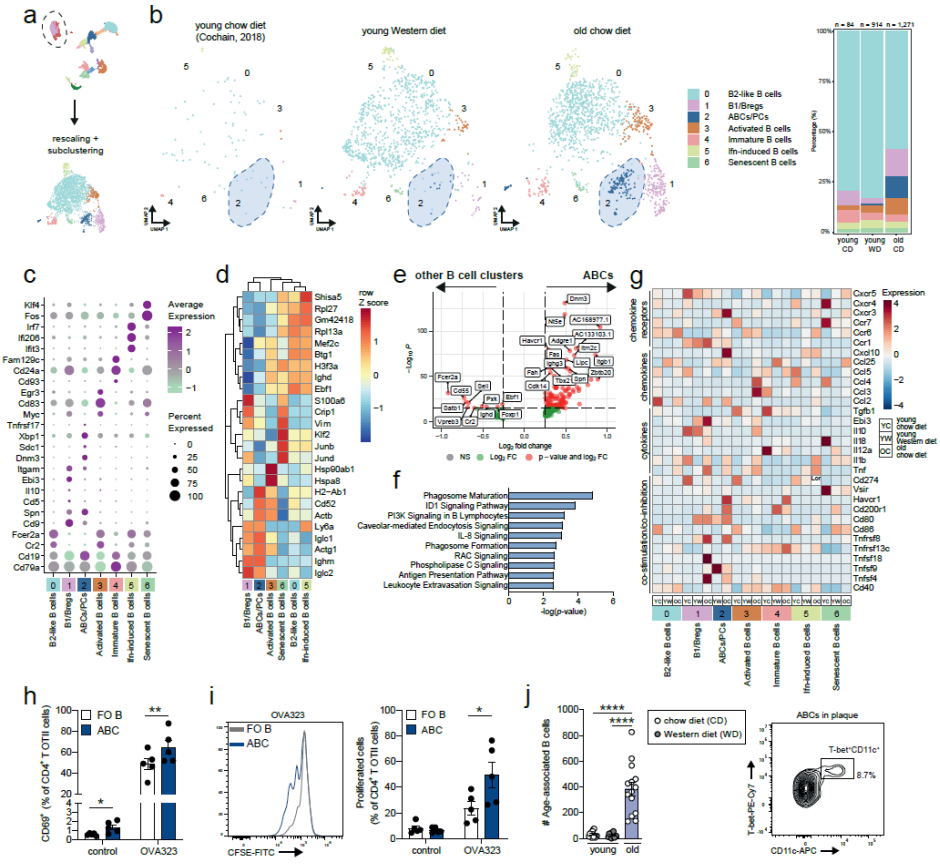

Figure 4. Characterization of age-associated B-cells in atherosclerotic aortas of *Ldlr*$^{-/-}$ mice.

a, *Cd79a*$^{+}$ clusters were extracted from the principal clustering and reclustered, after which the B-cells clusters were identified. **b**, UMAP plots and stacked diagrams visualizing the identified B-cell subclusters, in which ABCs are encircled in the dashed blue shape. **c**, Dot plot showing the average expression of immune cell cluster-defining markers for each cluster. **d**, Heatmap of hierarchically clustered top 25 variable genes across B-cell subclusters. **e**, Volcano plot of the differentially expressed genes (DEGs) in the age-associated B-cells (ABCs), excluded of plasma cells (PCs), compared to other B-cells in the B-cell subclustering. **f**, Top canonical pathways of the ABCs. **g**, Heatmap showing average expression of biological process-associated genes in B-cell clusters of young CD, young WD and old CD *Ldlr*$^{-/-}$ aortas. **h**, ABCs and follicular (FO) B-cells were tested for their capability to present OVA323 peptide antigen to CD4^{+} OTII T-cells and induce T-cell activation (CD69^{+}) or **i**, proliferation (n=5). **j**, Absolute numbers of CD19^{+}CD11b^{+}CD11c^{+} ABCs and representative plot of associated protein expression of CD11c and T-bet within the ABCs in aortas of *Ldlr*$^{-/-}$ mice (n=12-15). Gating strategy is shown in Supplementary material Figure S5a. Statistical significance was tested by two-tailed paired t-test (FO B-cells vs. ABCs) or one-way ANOVA (3 groups). Mean ± SEM plotted. *P<0.05, **P<0.01, ****P<0.0001.

Integrated analysis of myeloid cells reveals enrichment of inflammatory macrophages in aged atherosclerotic aortas

Myeloid populations such as dendritic cells and macrophages have been described as major players in atherosclerosis.[43] To assess age-induced changes within the myeloid cells, we reclustered the myeloid repertoire at higher resolution, resulting in 12 distinctive myeloid subpopulations (Figure 5a-b).

Cluster 0 and 8 holds M1-like *Il1b*$^{+}$ macrophages that showed high expression of proinflammatory markers, such as *Il1b* and *Nlrp3*, in addition to the gene encoding triggering receptor expressed on myeloid cells 1 (*Trem1*; Figure 5c).[44] Interestingly, expression of genes encoding pro-inflammatory chemokines and cytokines (*Cxcl2*, *Cxcl3*, *Il1a*, *Il1b*, *Il18*, *Tnf*) was decreased in aged compared to young macrophages clusters 0 and 8. In contrast, expression of extracellular matrix degrading metalloprotease (MMP) 9 was increased in aged *Il1b*^{hi} and *Nlrp3*^{hi} macrophages, suggesting an age-induced shift in functionality (Figure 5e).

Cluster 3, 4 and 7 show an M2-like macrophage signature with a common expression of *Trem2*, *Apoe* and genes encoding complement C1q chains (*C1qa, C1qb, C1qc*) (Figure 5c-d).[41] *Lyve1*$^{+}$*Mrc1*$^{+}$ resident macrophages[9,45] (cluster 7) were the main immune cell population in aortas of young CD mice (Figure 5c). *Trem2*$^{+}$ macrophages in cluster 4 displayed high expression of genes including *Abcg1*, *Fabp4*, *Fabp5*, *Spp1*, *Lgals3,* and *Apoe,* indicative of foamy macrophages[44,46], which were absent in aortas of young CD mice, present in young WD mice, but relatively decreased in old CD mice (Figure 5b and Supplementary material Figure S7b). Upon aging, genes related to antigen presentation and activation (e.g. *H2-Aa, H2-Ab1, Cd86*) were increased in the resident macrophages (Figure 5e), but not in *Trem2*^{hi} macrophages. In addition, expression of MMP-12 was upregulated with age in the *Trem2*^{hi} (foamy) macrophage clusters 3 and 4, although tissue inhibitor of MMPs (TIMP) 2, encoded by *Timp2*, was also upregulated in these clusters (Figure 5e). Considering the phagocytic capacity of macrophages, macrophages from aged *Ldlr*$^{-/-}$ mice express more recognition receptors important for efferocytosis (e.g. *Stab1*, *Timd4*) while expression of genes involved in engulfment (e.g. *Abca1*, *Rac1*, *Elmo1*) was decreased compared to that in young macrophages (Figure 5e)[47], suggesting an age-induced change in phagocytic capacity. To test age-related effects on macrophage phagocytosis, we skewed bone marrow-derived macrophages (BMDMs) from young and aged *Ldlr*$^{-/-}$ mice towards an M1- or M2-like phenotype and tested in vitro phagocytic function. Although apoptotic cell uptake was not altered upon aging, lipid uptake (% BODIPY^{+} cells) was decreased in aged compared to young M2-like BMDMs (Figure 5f-g and Supplementary material Figure S7c). The latter observation is in line with our scRNA-seq data, which showed a decrease in engulfment-related genes that could lead to decreased lipid uptake.

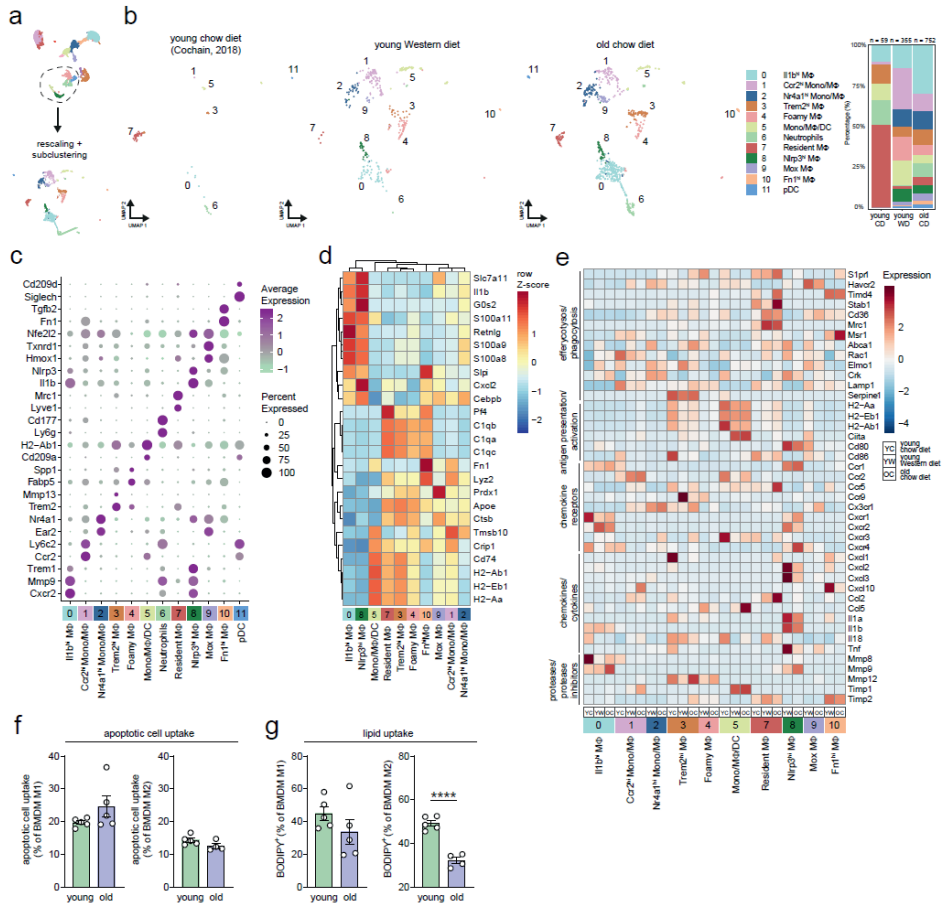

Figure 5. Integrated analysis of myeloid cells reveals age-induced phenotype alterations in macrophage subpopulations in atherosclerotic aortas.

a, *Cd68*$^{+}$ and *Itgam*$^{+}$ clusters were extracted from the principal clustering and reclustered, after which the myeloid clusters were identified. **b**, UMAP plots and stacked diagrams visualizing the identified myeloid subclusters. **c**, Dot plot showing the average expression of immune cell cluster-defining markers for each cluster. **d**, Dendrogram heatmap based on the 25 most differentially expressed genes from all macrophage clusters. **e,** Heatmap showing average expression of biological process-associated genes in myeloid cell clusters of young CD, young WD and old CD *Ldlr*$^{-/-}$ aortas. **f-g**, Percentage of M1- or M2-like bone marrow-derived macrophages (BMDM) of young and aged *Ldlr*$^{-/-}$ mice (n=5), that have taken up apoptotic cells (**f**) or BODIPY-labeled cholesteryl lipids (**g**), was measured by flow cytometry, of which the gating strategy is shown in Supplementary material Figure S7c. Statistical significance was tested by one-way ANOVA. Mean ± SEM plotted. ***P<0.001, ****P<0.0001.

Besides the *Il1b*$^{+}$ and *Trem2*$^{+}$ macrophage subsets, we also identified a population resembling Mox macrophages in cluster 9.[48] These macrophages were characterized by high expression of Nrf2 (encoded by *Nfe2l2*), a transcription factor that activates genes involved in synthesis of antioxidant enzymes in response to oxidative stress, and co-expression of antioxidant-associated genes *Hmox*, *Txnrd1* and *Cebpb* (Figure 5c).[48] In cluster 10, we detected macrophages with high expression of fibronectin (*Fn1*). Furthermore, we observed possibly recently recruited *Ly6c2*^{hi} monocytes and/or macrophages with high expression of *Ccr2* and *Fn1* in cluster 1. Cluster

2 contained *Ly6c2*^{lo} monocytes and/or macrophages expressing *Nr4a1* and *Ear2*, which have been described to have anti-atherogenic properties.[9] Cluster 5 contains a mix of monocytes, macrophages and DCs (*Cd209a*, *Flt3*, *Klrd1*; Figure 5c, Table S4), with high expression of genes encoding for MHCII (*H2-Ab1*, *H2-Aa*, *H2-Eb1*; Figure 5d). In contrast to the *Trem2*$^{+}$ macrophages, cluster 5 exhibits reduced expression of antigen presentation-associated genes in aged compared to young mice (Figure 5e), which is in line with a transcriptomic profiling study describing an age-associated downregulation of antigen-presentation pathways in human DCs.[49] Finally, we recovered two non-macrophage myeloid clusters from the principal clustering that were characterized as neutrophils (cluster 6) and pDCs (cluster 11; Figure 5c).

To summarize, aging affects the myeloid compartment in the atherosclerotic aorta by inducing a relative increase in *Il1b*$^{+}$ macrophages, by upregulating macrophage-derived MMP expression, and by altering antigen-presentation and phagocytosis-associated gene signatures.

Projection of scRNA-seq analysis of vascular leukocytes in healthy aortas onto atherosclerotic aortas

Additionally, we projected scRNA-seq data of healthy non-atherosclerotic aortas from young and aged C57BL/6 mice[15] onto our scRNA-seq data of *Ldlr*$^{-/-}$ aortas (Supplementary material Figure S8). Few immune cells are residing in the arterial wall of C57BL/6 aortas, which consisted mostly of *Cd68*- and *Itgax*-expressing myeloid cells that belong to cluster 4 (*Trem2*^{hi} macrophages), 6 (mixed myeloid cells I) and 11 (mixed myeloid cells II), while T- and B-cells were less present (Supplementary material Figure S8b-c).

Age-associated T and B-cells are present in human atherosclerotic plaques

Using scRNA-seq we have reported transcriptomic immune cell alterations in the aged aorta of *Ldlr*$^{-/-}$ mice, including the presence of age-associated cell subsets. To translate our findings and explore the relevance of Gzmk^{+}CD8^{+} T-cells in human atherosclerosis, we utilized a single-cell transcriptome dataset of 18 human plaques.[12] Granzyme K was mostly expressed in the largest T-cell cluster, namely CD3^{+}CD8^{+} T-cells, and similar to Gzmk^{+}CD8^{+} T-cells in aged mice, these cells expressed *EOMES*, *TOX*, *PDCD1* (PD-1), and *LAG3* (Figure 6a). Furthermore, we confirmed the presence of Gzmk^{+}TOX^{+}CD8^{+} T-cells with high expression of PD-1, in human atherosclerosis using flow cytometry (Figure 6b and Supplementary material Figure S9a), of which plaques showed higher levels of Gzmk^{+}TOX^{+}CD8^{+} T-cells within the CD8+ T-cells (33.3±4.6%) as compared to blood (20.1±3.1%, P<0.01). Finally, we confirmed the presence of ABCs, based on the expression of CD11b, CD11c and T-bet, in human atherosclerotic plaques and peripheral blood mononuclear cells (PBMCs) obtained from patients that underwent carotid endarterectomy (~71 years old, Figure 6c and Supplementary material Figure S9b) using flow cytometry. Intriguingly, we observed significantly increased levels of

ABCs within the B-cell compartment in the plaque (82.9±6.1%) compared to the circulation (27.7±7.4%, *P*<0.0001). In addition, human atherosclerotic plaques exhibited increased levels of T-bet$^+$ ABCs compared to PBMCs, which can be a consequence of tissue residency and the pro-inflammatory microenvironment in the plaque.[50,51]

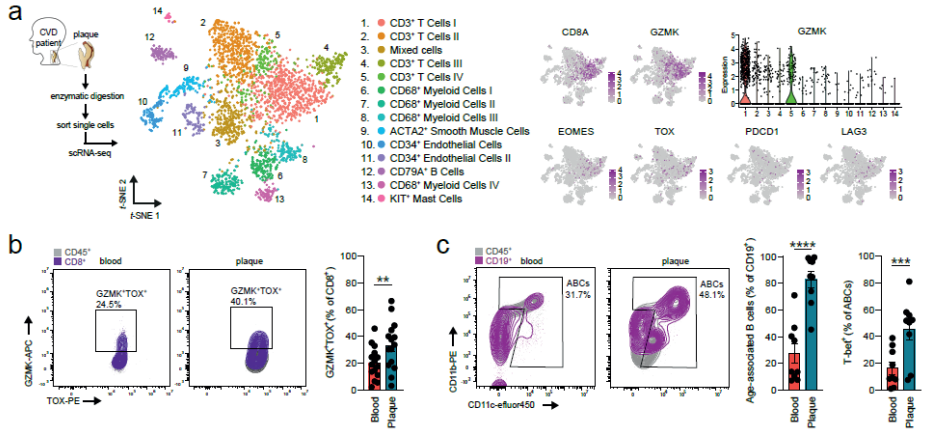

Figure 6. Flow cytometry analysis confirms expansion of age-associated T- and B-cells in human atherosclerotic plaques. **a**, Single-cell RNA sequencing analysis of human atherosclerotic plaques (n=18)[12], in which gene expression of GzmK$^+$ CD8 T-cell-associated markers *GZMK*, *EOMES*, *TOX*, *PDCD1* and *LAG3* are shown. **b**, Representative plot and quantification of GZMK$^+$TOX$^+$ as percentage of CD8$^+$ T-cells as measured in human atherosclerotic plaques and corresponding blood samples (n=15) with flow cytometry. **c**, Representative plot and quantification of CD11b$^+$CD11c$^+$ ABCs as percentage of B-cells, and expression of T-bet within ABCs measured in human atherosclerotic plaques and corresponding blood samples (n=9) with flow cytometry. Gating strategies are shown in Supplementary material Figure S9. Statistical significance was tested two-tailed paired t-test. Mean ± SEM plotted. **P<0.01, ***P<0.001, ****P<0.0001.

DISCUSSION

Healthy aging is one of the prime goals in today's society and atherosclerosis is among the greatest causes of morbidity in elderly. In order to gain better insights into age-driven atherosclerosis and to move one step closer towards tailored immunotherapies, research generating in-depth characterization of systemic and local inflammation in the atherosclerotic plaque upon aging is needed. Although several studies used state-of-the-art proteomic and transcriptomic approaches to identify cell subsets in murine atherosclerotic plaques[8,9,52,53], the translational aspect is limited as these were obtained from young mice, which do not display age-associated immunity. Our study provides, to our knowledge, the first comprehensive analysis of immunity in aged atherosclerotic mice, reporting a systemic myeloid skewing, enhanced effector (memory) phenotypes in T-cells, and the emergence of age-associated, pro-inflammatory immune cells in the atherosclerotic aorta. Moreover, presence of these age-associated immune cells was confirmed in CVD patients.

In contrast to the rapid development of atherosclerosis in young *Apoe*$^{-/-}$ mice or *Ldlr*$^{-/-}$ mice fed a Western diet, atherosclerosis is a slow process taking decades to develop and progress into advanced atherosclerotic plaques that eventually can cause acute cardiovascular events. Simultaneously, our immune system undergoes numerous changes as we age, including myeloid skewing and a functional decline in our protective immunity, which might affect atherosclerosis progression, plaque composition, and the efficacy of immunotherapies. By using naturally aged *Ldlr*$^{-/-}$ mice, which have mildly elevated cholesterol levels, both gradual plaque development and immunosenescence are accounted for, thereby resembling disease progression in humans. We observed age-associated alterations, such as elevated circulating monocytes, reduced levels of CD4^{+} and CD8^{+} T-cells, and a shift from naïve towards effector (memory) T-cells. Although the numerical decline of CD4 T-cells is more subtle in humans upon aging compared to mice[54], age-induced changes within the T-cell compartment, including reduced naïve T-cells, increased memory T-cells and the arise of age-associated Gzmk^{+}CD8^{+} T-cells occur in both.[24,55] Additionally, we found increased regulatory and effector T-cells upon activation, particularly pro-atherogenic IFNγ-producing T-cells, in our naturally aged atherosclerotic *Ldlr*$^{-/-}$ mice. This corroborates with a recent study by Elyahu et al. who showed a similar shift towards a more extreme effector T-cell phenotype within the splenic CD4^{+} T-cell compartment of old C57BL/6 mice, supporting a detrimental role for aged T-cells in inflammaging and immunosenescence.[56] The age-associated systemic changes can subsequently contribute to plaque growth and alter plaque composition.

In line with transcriptomic and proteomic data of human plaques obtained from aged CVD patients[12,57], T-cell clusters dominated aortic leukocytes in the aorta. Retrieval of conventional T helper cell subsets in the atherosclerotic plaque using scRNA-seq is difficult as we and others were unable to identify separate clusters of Th1/Th2/Th17 cells due to limited detection of their hallmark transcription factors and cytokines. However, we did observe a CD4^{+} T-cell cluster that mainly contains Tregs. Splenic and lymphoid Tregs from aged C57BL/6 mice showed enhanced release of IL-10, compared to Tregs from young mice[58], which we also observed in our aged *Ldlr*$^{-/-}$ mice. Although we could not detect IL-10 on mRNA level in the aorta, we found that Tregs from aged aortas show increased expression of Treg-related genes encoding suppressor cytokines TGF-β and IL-35, compared to Tregs from young aortas, confirming an enhanced regulatory phenotype, and could contribute to enhanced collagen deposition that we observed in lesions of aged atherosclerotic mice.[59,60] Interestingly, we identified a relatively large population of CD8^{+} T-cells in the aged aortic arch with enriched exhaustion markers, which mostly expressed *Gzmk* and *Eomes*. Recently, GzmK^{+} CD8^{+} T-cells were shown to expand in mice and humans with age and disease, as these cells are enriched in inflamed tissues of patients with rheumatoid arthritis (RA), inflammatory bowel disease, systemic lupus erythematosus (SLE), and coronavirus disease 2019 (COVID-19).[24,61] More importantly, we and others show that Gzmk^{+} CD8^{+} T-cells are abundant in atherosclerotic plaques of CVD

patients.[12,57] Although GzmK$^+$ CD8$^+$ T-cells express exhaustion markers, studies have shown that these cells are potent effector cells through secretion of IFN-γ, CCL5 and GzmK, of which the latter can promote release of pro-inflammatory senescence-associated secretory phenotype (SASP) components (e.g. IL-6, CCL2, and CXCL1) by senescent cells.[24,61] Presence of these cells locally in the atherosclerotic plaque may contribute to enhanced inflammation.

We also found a relatively large amount of B-cells in the aged *Ldlr*$^{-/-}$ aorta and were able to identify a wide variety of B-cell subsets. The largest cluster was formed by B-cells resembling B2-cells which are known to aggravate atherosclerosis[27] and are also the predominant B-cell subset found in young aortas.[8,62] The relative increase of B-cells in aortic leukocytes of aged *Ldlr*$^{-/-}$ mice could be ascribed to the expansion of CD21^{low} B-cells, that exhibited enhanced activation, as illustrated by elevated expression of genes encoding co-stimulatory/inhibitory molecules, cytokines and chemokines. Within these CD21^{low} B-cells, we identified B-cells with previously described anti-atherogenic features including CD9$^+$CD43$^+$ B1-like cells and IL-10$^+$ regulatory B-cells.[63] B1-cells have also been reported to give rise to pro-atherogenic GM-CSF$^+$ IRA B-cells[64], but we did not find *Csf2* (GM-CSF) expression in this cluster. Most interestingly, we identified CD21^{low}CD11b$^+$CD11c$^+$T-bet$^+$ ABCs in aged aortas, that are superior in antigen- presentation and T-cell activation compared to follicular B2-cells. ABCs are known to accumulate with age and autoimmune diseases[33,34], but up to date have not been described in atherosclerosis. As CD-fed young *Ldlr*$^{-/-}$ and C57BL/6 mice barely have any atherosclerosis, not surprisingly, scRNA-seq of these healthy C57BL/6 aortas revealed low numbers of immune cell reads. Although this forms a limitation in comparing the data, we supported our scRNA-seq deducted findings with flow cytometry data of ABCs in aortas of *Ldlr*$^{-/-}$ mice and C57BL/6 mice, showing that accumulation of ABCs in the aortic environment of *Ldlr*$^{-/-}$ mice is co-dependent on aging and atherosclerosis. ABCs are driven by IL-21, IFN-γ, and Toll-like receptor (TLR) 7 and 9 activation (e.g. via self-nucleic acids), after which they secrete pro-inflammatory cytokines (e.g. IL-6, IL-1β, and TNF-α) and high levels of autoantibodies.[65] Indeed, we found elevated gene expression levels of IL-1β and TNF-α, plasma cell differentiation-associated gene *Zbtb20*, and T-bet expression (associated with autoantibody production)[66] in the ABC cluster, which supports the pro-inflammatory cytokine and antibody-producing potential of these cells. Previous studies have shown that ABCs exert a pathogenic role in chronic diseases, such as RA, SLE and Crohn's disease.[67,68] We now show that ABCs are present in CVD patients and are relatively enriched in carotid human plaques compared to the circulation. Possibly, systemic inflammaging and the microenvironment of the atherosclerotic plaque containing debris from damaged and dead cells, promote commitment of B-cells to this ABC fate in atherosclerosis, but the exact contribution of ABCs to atherosclerosis is currently under investigation.

Furthermore, we identified distinctive macrophage subsets, including pro-inflammatory *Il1b*$^+$ macrophages and *Trem2*$^+$ macrophages.[44,69] Macrophages in the aged aorta expressed increased

levels of genes encoding MMPs (MMP-9 and 12), although *Mmp12* upregulation in clusters 3 and 6 could be counteracted by upregulated *Timp2* co-expression.[70] MMPs are generally associated with plaque instability by degradation of extracellular matrix components (e.g. collagen).[71] However, some studies have also reported that MMPs promote collagen deposition in plaques through TGF-β activation[72,73], in addition to increased vascular calcification.[74] Increased expression levels of macrophage-derived MMPs in atherosclerotic aortas of aged mice could therefore be associated with the increased collagen content and calcification within the atherosclerotic plaque upon aging, but this should be confirmed with further research on protein level. Notably, previous studies have shown that non-immune cells, such as vascular smooth muscle cells, are known to increase collagen deposition with age[75] and can thereby also contribute to the collagen-rich plaque environment in aged *Ldlr*$^{-/-}$ mice. Defects in phagocytosis and efferocytosis have been observed in macrophages of aged individuals.[76] In our data, we show that aging affects lipid-uptake by M2-like macrophages in *Ldlr*$^{-/-}$ mice.

Collectively, we provide comprehensive profiling of aged immunity in atherosclerotic mice, enhancing our knowledge on the pathophysiology of atherosclerosis. Our results stress the importance of taking age into account when aiming to halt progression of atherosclerotic plaques, as we reveal the emergence of specific age-associated T- and B-cell subsets in the atherosclerotic aorta of aged mice and in atherosclerotic plaques and blood of CVD patients. Where the age-associated cells are precisely located in the atherosclerotic plaque environment remains to be investigated. Future research investigating mechanisms underlying the activation, accumulation and function of age-associated cells in experimental atherosclerosis and CVD patients, will further enhance our understanding of disease etiology and can serve as a foundation for diagnostic and therapeutic strategies to combat cardiovascular disease.

FUNDING

This work was supported by the Dutch Heart Foundation grant number 2018T051 to A.C.F., 2019T067 to I.B., CVON2017-20: Generating the best evidence-based pharmaceutical targets and drugs for atherosclerosis (GENIUS II) to J.K, and the ERA-CVD B-eatATHERO consortium; Dutch Heart Foundation grant number 2019T107 to A.C.F., Austrian Science Fund (FWF) grant number I4647 to D.T., and the Leducq Foundation grant number TNE-20CVD03 to C.J.B.

ACKNOWLEDGEMENTS

We would like to thank Berend from the *Flow Cytometry Core Facility* and Marja from the *Genomics Core Facility* of the AMC for flow sorting and processing the samples for sequencing. We would also like to thank Dr. S. Semrau for his advice on scRNA-seq data processing, and Pien Killiaan and Maria Ozsvar Kozma for technical help. Graphical abstract was created with BioRender.com.

AUTHOR CONTRIBUTIONS

V.S. and A.C.F. participated in the conceptualization, performed data analysis, drafted the manuscript, and designed the figures. V.S., J.d.M., F.H.S., M.A.C.D., R.J.P., D.S., J.v.D., R.A.F.V., H.W.G., E.v.I., M.J.M.d.J., M.N.A.B.K., I.B., and A.C.F executed the animal experiments. L.G., J.A.H.M.P., H.J.S. and A.W. performed carotid endarterectomy procedures and human sample collection at the HMC. V.S. and M.A.C.D. performed FACS and flow cytometry. V.S. performed the scRNA-seq analysis. F.H.S., F.W.M.V., L.B. and A.C.F. contributed to the scRNA-seq clustering analysis. V.S., F.W.M.V., L.B., J.K., M.P.J.d.W., J.d.M., J.K.P., D.T., and A.C.F. contributed to the interpretation of the scRNA-seq data. C.J.B. contributed to the antibody measurements. All authors provided feedback on the research, analyses and manuscript.

DISCLOSURES

The authors have no conflicts of interest.

SUPPLEMENTARY MATERIAL

Detailed Methods
Supplementary Figures 1-9
Supplementary Tables 1-4
Major Resources Table

REFERENCES

1. Nikolich-Žugich J. Aging of the T Cell Compartment in Mice and Humans: From No Naive Expectations to Foggy Memories. *The Journal of Immunology* 2014;**193**:2622–2629.
2. Ho YH, Toro R del, Rivera-Torres J, Rak J, Korn C, García-García A, Macías D, González-Gómez C, Monte A del, Wittner M, Waller AK, Foster HR, López-Otín C, Johnson RS, Nerlov C, Ghevaert C, Vainchenker W, Louache F, Andrés V, Méndez-Ferrer S. Remodeling of Bone Marrow Hematopoietic Stem Cell Niches Promotes Myeloid Cell Expansion during Premature or Physiological Aging. *Cell Stem Cell* 2019;**25**:407-418.e6.
3. Nikolich-Žugich J. The twilight of immunity: Emerging concepts in aging of the immune system review-article. *Nat Immunol* 2018;**19**:10–19.
4. Franceschi C, Bonafè M, Valensin S, Olivieri F, Luca M de, Ottaviani E, Benedictis G de. Inflamm-aging. An evolutionary perspective on immunosenescence. *Ann N Y Acad Sci* 2000;**908**:244–254.
5. Goronzy JJ, Li G, Yang Z, Weyand CM. The janus head of T cell aging – autoimmunity and immunodeficiency. *Front Immunol* 2013;**4**:131.
6. Global Burden of Disease Collaborative Network. Global Burden of Disease Study 2017 Results
7. Witztum JL, Lichtman AH. The Influence of Innate and Adaptive Immune Responses on Atherosclerosis. *Annual Review of Pathology: Mechanisms of Disease* 2014;**9**:73–102.
8. Winkels H, Ehinger E, Vassallo M, Buscher K, Dinh HQ, Kobiyama K, Hamers AAJ, Cochain C, Vafadarnejad E, Saliba AE, Zernecke A, Pramod AB, Ghosh AK, Michel NA, Hoppe N, Hilgendorf I, Zirlik A, Hedrick CC, Ley K, Wolf D. Atlas of the immune cell repertoire in mouse atherosclerosis defined by single-cell RNA-sequencing and mass cytometry. *Circ Res* 2018;**122**:1675–1688.
9. Cochain C, Vafadarnejad E, Arampatzi P, Pelisek J, Winkels H, Ley K, Wolf D, Saliba AE, Zernecke A. Single-cell RNA-seq reveals the transcriptional landscape and heterogeneity of aortic macrophages in murine atherosclerosis. *Circ Res* 2018;**122**:1661–1674.
10. Okunrintemi V, Tibuakuu M, Virani SS, Sperling LS, Volgman AS, Gulati M, Cho L, Leucker TM, Blumenthal RS, Michos ED. Sex differences in the age of diagnosis for cardiovascular disease and its risk factors among us adults: Trends from 2008 to 2017, the medical expenditure panel survey. *J Am Heart Assoc* 2020;**9**.
11. Gruber S, Hendrikx T, Tsiantoulas D, Ozsvar-Kozma M, Göderle L, Mallat Z, Witztum JL, Shiri-Sverdlov R, Nitschke L, Binder CJ. Sialic Acid-Binding Immunoglobulin-like Lectin G Promotes Atherosclerosis and Liver Inflammation by Suppressing the Protective Functions of B-1 Cells. *Cell Rep* 2016;**14**:2348–2361.
12. Depuydt MAC, Prange KHM, Slenders L, Örd T, Elbersen D, Boltjes A, Jager SC de, Asselbergs FW, Borst GJ de, Aavik E, Lönnberg T, Lutgens E, Glass CK, Ruijter HM den, Kaikkonen MU, Bot I, Slütter B, Laan SW van der, Yla-Herttuala S, Mokry M, Kuiper J, Winther MPJ de, Pasterkamp G. Microanatomy of the Human Atherosclerotic Plaque by Single-Cell Transcriptomics. *Circ Res* 2020.
13. Douna H, Amersfoort J, Schaftenaar FH, Kröner MJ, Kiss MG, Slütter B, Depuydt MAC, Bernabé Kleijn MNA, Wezel A, Smeets HJ, Yagita H, Binder CJ, Bot I, Puijvelde GHM van, Kuiper J, Foks AC. B- And T-lymphocyte attenuator stimulation protects against atherosclerosis by regulating follicular B cells. *Cardiovasc Res* 2020;**116**:295–305.
14. DePasquale EAK, Schnell DJ, Camp PJ van, Valiente-Alandí Í, Blaxall BC, Grimes HL, Singh H, Salomonis N. DoubletDecon: Deconvoluting Doublets from Single-Cell RNA-Sequencing Data. *Cell Rep* 2019;**29**:1718-1727.e8.
15. Tabula Muris Consortium. A single-cell transcriptomic atlas characterizes ageing tissues in the mouse. *Nature* 2020;**583**:590–595.

16. Frasca D, Diaz A, Romero M, Blomberg BB. The generation of memory B cells is maintained, but the antibody response is not, in the elderly after repeated influenza immunizations. *Vaccine* 2016;**34**:2834–2840.
17. Hume DA, Summers KM, Raza S, Baillie JK, Freeman TC. Functional clustering and lineage markers: Insights into cellular differentiation and gene function from large-scale microarray studies of purified primary cell populations. *Genomics* 2010;**95**:328–338.
18. Saigusa R, Winkels H, Ley K. T cell subsets and functions in atherosclerosis. *Nat Rev Cardiol* 2020;**17**:387–401.
19. Mingueneau M, Kreslavsky T, Gray D, Heng T, Cruse R, Ericson J, Bendall S, Spitzer MH, Nolan GP, Kobayashi K, Boehmer H von, Mathis D, Benoist C, Best AJ, Knell J, Goldrath A, Koller D, Shay T, Regev A, Cohen N, Brennan P, Brenner M, Kim F, Rao TN, Wagers A, Rothamel K, Ortiz-Lopez A, Bezman NA, Sun JC, Min-Oo G, Kim CC, Lanier LL, Miller J, Brown B, Merad M, Gautier EL, Jakubzick C, Randolph GJ, Monach P, Blair DA, Dustin ML, Shinton SA, Hardy RR, Laidlaw D, Collins J, Gazit R, Rossi DJ, Malhotra N, Sylvia K, Kang J, Fletcher A, Elpek K, Bellemare-Pelletier A, Malhotra D, Turley S. The transcriptional landscape of αβ T cell differentiation. *Nat Immunol* 2013;**14**:619–632.
20. Winkels H, Ghosheh Y, Kobiyama K, Kiosses WB, Orecchioni M, Ehinger E, Suryawanshi V, Herrera-De La Mata S, Marchovecchio P, Riffelmacher T, Thiault N, Kronenberg M, Wolf D, Seumois G, Vijayanand P, Ley K. Thymus-Derived CD4 + CD8 + Cells Reside in Mediastinal Adipose Tissue and the Aortic Arch . *The Journal of Immunology* 2021;**207**:2720–2732.
21. Kirchner J, Bevan MJ. ITM2A is induced during thymocyte selection and T cell activation and causes downregulation of CD8 when overexpressed in CD4+CD8+ double positive thymocytes. *Journal of Experimental Medicine* 1999;**190**:217–228.
22. Aliahmad P, Seksenyan A, Kaye J. The many roles of TOX in the immune system. *Curr Opin Immunol* 2012;**24**:173–177.
23. Ricardo Miragaia AJ, Gomes T, Chomka A, Haniffa M, Powrie F, Teichmann SA. Single-Cell Transcriptomics of Regulatory T Cells Reveals Trajectories of Tissue Adaptation. *Immunity* 2019;**50**:493–504.
24. Mogilenko DA, Shpynov O, Andhey PS, Arthur L, Swain A, Esaulova E, Brioschi S, Shchukina I, Kerndl M, Bambouskova M, Yao Z, Laha A, Zaitsev K, Burdess S, Gillfilan S, Stewart SA, Colonna M, Artyomov MN. Comprehensive Profiling of an Aging Immune System Reveals Clonal GZMK+ CD8+ T Cells as Conserved Hallmark of Inflammaging. *Immunity* 2020;**54**:99-115.e12.
25. Welsh GI, Miyamoto S, Priced NT, Safer B, Proud CG. T-cell activation leads to rapid stimulation of translation initiation factor eIF2B and inactivation of glycogen synthase kinase-3. *J Biol Chem* 1996;**271**:11410–11413.
26. Ribot JC, deBarros A, Pang DJ, Neves JF, Peperzak V, Roberts SJ, Girardi M, Borst J, Hayday AC, Pennington DJ, Silva-Santos B. CD27 is a thymic determinant of the balance between interferon-γ- and interleukin 17-producing γδ T cell subsets. *Nat Immunol* 2009;**10**:427–436.
27. Sage AP, Tsiantoulas D, Binder CJ, Mallat Z. The role of B cells in atherosclerosis. *Nat Rev Cardiol* 2019;**16**:180–196.
28. Fowler T, Garruss AS, Ghosh A, De S, Becker KG, Wood WH, Weirauch MT, Smale ST, Aronow B, Sen R, Roy AL. Divergence of transcriptional landscape occurs early in B cell activation. *Epigenetics Chromatin* 2015;**8**:1–14.
29. Sun J, Wang J, Pefanis E, Chao J, Rothschild G, Tachibana I, Chen JK, Ivanov II, Rabadan R, Takeda Y, Basu U. Transcriptomics Identify CD9 as a Marker of Murine IL-10-Competent Regulatory B Cells. *Cell Rep* 2015;**13**:1110–1117.

30. Dambuza IM, He C, Choi JK, Yu CR, Wang R, Mattapallil MJ, Wingfield PT, Caspi RR, Egwuagu CE. IL-12p35 induces expansion of IL-10 and IL-35-expressing regulatory B cells and ameliorates autoimmune disease. *Nat Commun* 2017;**8**:1–12.
31. Thompson MR, Xu D, Williams BRG. ATF3 transcription factor and its emerging roles in immunity and cancer. *J Mol Med* 2009;**87**:1053–1060.
32. Masle-Farquhar E, Peters TJ, Miosge LA, Parish IA, Weigel C, Oakes CC, Reed JH, Goodnow CC. Uncontrolled CD21low age-associated and B1 B cell accumulation caused by failure of an EGR2/3 tolerance checkpoint. *Cell Rep* 2022;**38**:110259.
33. Rubtsov A v., Rubtsova K, Fischer A, Meehan RT, Gillis JZ, Kappler JW, Marrack P. Toll-like receptor 7 (TLR7)-driven accumulation of a novel CD11c+ B-cell population is important for the development of autoimmunity. *Blood* 2011;**118**:1305–1315.
34. Hao Y, O'Neill P, Naradikian MS, Scholz JL, Cancro MP. A B-cell subset uniquely responsive to innate stimuli accumulates in aged mice. *Blood* 2011;**118**:1294–1304.
35. Cancro MP. Age-Associated B Cells. *Annu Rev Immunol* 2020;**38**:315–340.
36. Knode LMR, Naradikian MS, Myles A, Scholz JL, Hao Y, Liu D, Ford ML, Tobias JW, Cancro MP, Gearhart PJ. Age-Associated B Cells Express a Diverse Repertoire of VH and Vκ Genes with Somatic Hypermutation. *The Journal of Immunology* 2017;**198**:1921–1927.
37. Rubtsov A v., Rubtsova K, Kappler JW, Jacobelli J, Friedman RS, Marrack P. CD11c-Expressing B Cells Are Located at the T Cell/B Cell Border in Spleen and Are Potent APCs. *The Journal of Immunology* 2015;**195**:71–79.
38. Gu C, Yao J, Sun P. Dynamin 3 suppresses growth and induces apoptosis of hepatocellular carcinoma cells by activating inducible nitric oxide synthase production. *Oncol Lett* 2017;**13**:4776–4784.
39. Minnich M, Tagoh H, Bönelt P, Axelsson E, Fischer M, Cebolla B, Tarakhovsky A, Nutt SL, Jaritz M, Busslinger M. Multifunctional role of the transcription factor Blimp-1 in coordinating plasma cell differentiation. *Nat Immunol* 2016;**17**:331–343.
40. Gou B, Chu X, Xiao Y, Liu P, Zhang H, Gao Z, Song M. Single-Cell Analysis Reveals Transcriptomic Reprogramming in Aging Cardiovascular Endothelial Cells. *Front Cardiovasc Med* 2022;**0**:1034.
41. Xu Q, Liu M, Zhang J, Xue L, Zhang G, Hu C, Wang Z, He S, Chen L, Ma K, Liu X, Zhao Y, Lv N, Liang S, Zhu H, Xu N, Xu Q, Liu M, Zhang J, Xue L, Zhang G, Hu C, Wang Z, He S, Chen L, Ma K, Liu X, Zhao Y, Lv N, Liang S, Zhu H, Xu N. Overexpression of KLF4 promotes cell senescence through microRNA-203-survivin-p21 pathway. *Oncotarget* 2016;**7**:60290–60302.
42. Tong LQ, Toliver-Kinsky T, Edwards M, Rassin DK, Werrbach-Perez K, Regino Perez-Polo J. Attenuated transcriptional responses to oxidative stress in the aged rat brain. *J Neurosci Res* 2002;**70**:318–326.
43. Koltsova EK, Hedrick CC, Ley K. Myeloid cells in atherosclerosis: A delicate balance of anti-inflammatory and proinflammatory mechanisms. *Curr Opin Lipidol* 2013;**24**:371–380.
44. Willemsen L, Winther MP. Macrophage subsets in atherosclerosis as defined by single-cell technologies. *J Pathol* 2020;**250**:705–714.
45. Lim HY, Lim SY, Tan CK, Thiam CH, Goh CC, Carbajo D, Chew SHS, See P, Chakarov S, Wang XN, Lim LH, Johnson LA, Lum J, Fong CY, Bongso A, Biswas A, Goh C, Evrard M, Yeo KP, Basu R, Wang JK, Tan Y, Jain R, Tikoo S, Choong C, Weninger W, Poidinger M, Stanley RE, Collin M, Tan NS, Ng LG, Jackson DG, Ginhoux F, Angeli V. Hyaluronan Receptor LYVE-1-Expressing Macrophages Maintain Arterial Tone through Hyaluronan-Mediated Regulation of Smooth Muscle Cell Collagen. *Immunity* 2018;**49**:326-341.e7.
46. Zernecke A, Erhard F, Weinberger T, Schulz C, Ley K, Saliba A-E, Cochain C. Integrated single-cell analysis-based classification of vascular mononuclear phagocytes in mouse and human atherosclerosis. *Cardiovasc Res* 2022.

47. Zhang W, Zhao J, Wang R, Jiang M, Ye Q, Smith AD, Chen J, Shi Y. Macrophages reprogram after ischemic stroke and promote efferocytosis and inflammation resolution in the mouse brain. *CNS Neurosci Ther* 2019;**25**:1329–1342.
48. Kadl A, Meher AK, Sharma PR, Lee MY, Doran AC, Johnstone SR, Elliott MR, Gruber F, Han J, Chen W, Kensler T, Ravichandran KS, Isakson BE, Wamhoff BR, Leitinger N. Identification of a novel macrophage phenotype that develops in response to atherogenic phospholipids via Nrf2. *Circ Res* 2010;**107**:737–746.
49. Rahmatpanah F, Agrawal S, Scarfone VM, Kapadia S, Mercola D, Agrawal A. Transcriptional Profiling of Age-Associated Gene Expression Changes in Human Circulatory CD1c+ Myeloid Dendritic Cell Subset. *The Journals of Gerontology: Series A* 2019;**74**:9–15.
50. Naradikian MS, Myles A, Beiting DP, Roberts KJ, Dawson L, Herati RS, Bengsch B, Linderman SL, Stelekati E, Spolski R, Wherry EJ, Hunter C, Hensley SE, Leonard WJ, Cancro MP. Cutting Edge: IL-4, IL-21, and IFN-γ Interact To Govern T-bet and CD11c Expression in TLR-Activated B Cells. *The Journal of Immunology* 2016;**197**:1023–1028.
51. Johnson JL, Rosenthal RL, Knox JJ, Myles A, Naradikian MS, Madej J, Kostiv M, Rosenfeld AM, Meng W, Christensen SR, Hensley SE, Yewdell J, Canaday DH, Zhu J, McDermott AB, Dori Y, Itkin M, Wherry EJ, Pardi N, Weissman D, Naji A, Prak ETL, Betts MR, Cancro MP. The Transcription Factor T-bet Resolves Memory B Cell Subsets with Distinct Tissue Distributions and Antibody Specificities in Mice and Humans. *Immunity* 2020;**52**:842-855.e6.
52. Kim K, Shim D, Lee JS, Zaitsev K, Williams JW, Kim K-W, Jang M-Y, Seok Jang H, Yun TJ, Lee SH, Yoon WK, Prat A, Seidah NG, Choi J, Lee S-P, Yoon S-H, Nam JW, Seong JK, Oh GT, Randolph GJ, Artyomov MN, Cheong C, Choi J-H. Transcriptome Analysis Reveals Nonfoamy Rather Than Foamy Plaque Macrophages Are Proinflammatory in Atherosclerotic Murine Models. *Circ Res* 2018;**123**:1127–1142.
53. Lin J da, Nishi H, Poles J, Niu X, Mccauley C, Rahman K, Brown EJ, Yeung ST, Vozhilla N, Weinstock A, Ramsey SA, Fisher EA, Loke P. Single-cell analysis of fate-mapped macrophages reveals heterogeneity, including stem-like properties, during atherosclerosis progression and regression. *JCI Insight* 2019;**4**.
54. Grievink HW, Smit V, Huisman BW, Gal P, Yavuz Y, Klerks C, Binder CJ, Bot I, Kuiper J, Foks AC, Moerland M. Cardiovascular risk factors: The effects of ageing and smoking on the immune system, an observational clinical study. *Front Immunol* 2022;**13**:5391.
55. Márquez EJ, Chung C han, Marches R, Rossi RJ, Nehar-Belaid D, Eroglu A, Mellert DJ, Kuchel GA, Banchereau J, Ucar D. Sexual-dimorphism in human immune system aging. *Nature Communications 2020 11:1* 2020;**11**:1–17.
56. Elyahu Y, Hekselman I, Eizenberg-Magar I, Berner O, Strominger I, Schiller M, Mittal K, Nemirovsky A, Eremenko E, Vital A, Simonovsky E, Chalifa-Caspi V, Friedman N, Yeger-Lotem E, Monsonego A. Aging promotes reorganization of the CD4 T cell landscape toward extreme regulatory and effector phenotypes. *Sci Adv* 2019;**5**:eaaw8330.
57. Fernandez DM, Rahman AH, Fernandez NF, Chudnovskiy A, Amir E ad D, Amadori L, Khan NS, Wong CK, Shamailova R, Hill CA, Wang Z, Remark R, Li JR, Pina C, Faries C, Awad AJ, Moss N, Bjorkegren JLM, Kim-Schulze S, Gnjatic S, Ma'ayan A, Mocco J, Faries P, Merad M, Giannarelli C. Single-cell immune landscape of human atherosclerotic plaques. *Nat Med* 2019;**25**:1576–1588.
58. Garg SK, Delaney C, Toubai T, Ghosh A, Reddy P, Banerjee R, Yung R. Aging is associated with increased regulatory T-cell function. *Aging Cell* 2014;**13**:441–448.
59. Foks AC, Frodermann V, Borg M ter, Habets KLL, Bot I, Zhao Y, Eck M van, Berkel TJC van, Kuiper J, Puijvelde GHM van. Differential effects of regulatory T cells on the initiation and regression of atherosclerosis. *Atherosclerosis* 2011;**218**:53–60.

60. Robertson AKL, Rudling M, Zhou X, Gorelik L, Flavell RA, Hansson GK. Disruption of TGF-β signaling in T cells accelerates atherosclerosis. *Journal of Clinical Investigation* 2003;**112**:1342.
61. Jonsson AH, Zhang F, Dunlap G, Gomez-Rivas E, Watts GFM, Faust HJ, Rupani KV, Mears JR, Meednu N, Wang R, Keras G, Coblyn JS, Massarotti EM, Todd DJ, Anolik JH, McDavid A, Wei K, Rao DA, Raychaudhuri S, Brenner MB. Granzyme K+ CD8 T cells form a core population in inflamed human tissue. *Sci Transl Med* 2022;**14**:eabo0686.
62. Kyaw T, Tay C, Khan A, Dumouchel V, Cao A, To K, Kehry M, Dunn R, Agrotis A, Tipping P, Bobik A, Toh B-H. Conventional B2 B Cell Depletion Ameliorates whereas Its Adoptive Transfer Aggravates Atherosclerosis. *The Journal of Immunology* 2010;**185**:4410–4419.
63. Douna H, Amersfoort J, Schaftenaar FH, Kroon S, Puijvelde GHM van, Kuiper J, Foks AC. Bidirectional effects of IL-10+ regulatory B cells in Ldlr−/− mice. *Atherosclerosis* 2019;**280**:118–125.
64. Hilgendorf I, Theurl I, Gerhardt LMS, Robbins CS, Weber GF, Gonen A, Iwamoto Y, Degousee N, Holderried TAW, Winter C, Zirlik A, Lin HY, Sukhova GK, Butany J, Rubin BB, Witztum JL, Libby P, Nahrendorf M, Weissleder R, Swirski FK. Innate response activator b cells aggravate atherosclerosis by stimulating t helper-1 adaptive immunity. *Circulation* 2014;**129**:1677–1687.
65. Phalke S, Rivera-Correa J, Jenkins D, Flores Castro D, Giannopoulou E, Pernis AB. Molecular mechanisms controlling age-associated B cells in autoimmunity*. *Immunol Rev* 2022;**307**:79–100.
66. Peng SL, Szabo SJ, Glimcher LH. T-bet regulates IgG class switching and pathogenic autoantibody production. *Proc Natl Acad Sci U S A* 2002;**99**:5545–5550.
67. Keller B, Strohmeier V, Harder I, Unger S, Payne KJ, Andrieux G, Boerries M, Felixberger PT, Landry JJM, Nieters A, Rensing-Ehl A, Salzer U, Frede N, Usadel S, Elling R, Speckmann C, Hainmann I, Ralph E, Gilmour K, Wentink MWJ, Burg M van der, Kuehn HS, Rosenzweig SD, Kölsch U, Bernuth H von, Kaiser-Labusch P, Gothe F, Hambleton S, Vlagea AD, Garcia AG, Alsina L, Markelj G, Avcin T, Vasconcelos J, Guedes M, Ding JY, Ku CL, Shadur B, Avery DT, Venhoff N, Thiel J, Becker H, Erazo-Borrás L, Trujillo-Vargas CM, Franco JL, Fieschi C, Okada S, Gray PE, Uzel G, Casanova JL, Fliegauf M, Grimbacher B, Eibel H, Ehl S, Voll RE, Rizzi M, Stepensky P, Benes V, Ma CS, Bossen C, Tangye SG, Warnatz K. The expansion of human T-bethighCD21low B cells is T cell dependent. *Sci Immunol* 2021;**6**:52.
68. Wang Z, Wang Z, Wang J, Diao Y, Qian X, Zhu N. T-bet-Expressing B Cells Are Positively Associated with Crohn's Disease Activity and Support Th1 Inflammation. *DNA Cell Biology* 2016;**35**:628–635.
69. Williams JW, Zaitsev K, Kim KW, Ivanov S, Saunders BT, Schrank PR, Kim K, Elvington A, Kim SH, Tucker CG, Wohltmann M, Fife BT, Epelman S, Artyomov MN, Lavine KJ, Zinselmeyer BH, Choi JH, Randolph GJ. Limited proliferation capacity of aortic intima resident macrophages requires monocyte recruitment for atherosclerotic plaque progression. *Nature Immunology 2020 21:10* 2020;**21**:1194–1204.
70. Johnson JL. Matrix metalloproteinases and their inhibitors in cardiovascular pathologies: current knowledge and clinical potential. *Metalloproteinases Med* 2014;**1**:21–36.
71. Li T, Li X, Feng Y, Dong G, Wang Y, Yang J. The Role of Matrix Metalloproteinase-9 in Atherosclerotic Plaque Instability. *Mediators Inflamm* 2020;**2020**.
72. Lemaître V, Kim HE, Forney-Prescott M, Okada Y, D'Armiento J. Transgenic expression of matrix metalloproteinase-9 modulates collagen deposition in a mouse model of atherosclerosis. *Atherosclerosis* 2009;**205**:107–112.
73. Johnson JL, George SJ, Newby AC, Jackson CL. Divergent effects of matrix metalloproteinases 3, 7, 9, and 12 on atherosclerotic plaque stability in mouse brachiocephalic arteries. *Proc Natl Acad Sci U S A* 2005;**102**:15575.

74. Chen NX, O'Neill KD, Chen X, Kiattisunthorn K, Gattone VH, Moe SM. Activation of Arterial Matrix Metalloproteinases Leads to Vascular Calcification in Chronic Kidney Disease. *Am J Nephrol* 2011;**34**:211–219.
75. Ribeiro-Silva JC, Nolasco P, Krieger JE, Miyakawa AA. Dynamic Crosstalk between Vascular Smooth Muscle Cells and the Aged Extracellular Matrix. *International Journal of Molecular Sciences 2021, Vol 22, Page 10175* 2021;**22**:10175.
76. Maeyer RPH de, Chambers ES. The impact of ageing on monocytes and macrophages. *Immunol Lett* 2021;**230**:1–10.

SUPPLEMENTARY MATERIAL

DETAILED METHODS

Animals

All animal experiments were approved by the Leiden University Animal Ethics Committee and were performed according to the guidelines of the European Parliament Directive 2010/63/EU of the European Parliament. Female C57BL/6J, *Ldlr*$^{-/-}$ and *Apoe*$^{-/-}$ mice (if not specified elsewhere: young, 3 months or aged, 20 months old), and OTII mice (4 months old) on a C57Bl/6J genetic background were bred and aged in-house and kept under standard laboratory conditions. Mice were randomized according to weight and basal serum cholesterol levels. C57BL/6J, and *Apoe*$^{-/-}$ and OTII mice were fed a regular chow diet (CD). Aged *Ldlr*$^{-/-}$ mice were fed a regular chow diet (CD), while young mice were fed a CD or a Western diet (WD) containing 0.25% cholesterol and 15% cocoa butter (Special Diet Services, Witham, Essex, UK) for 10 weeks. Diet and water were provided *ad libitum*. During the experiment, health status of the mice was assessed weekly by body condition scoring. At the end of experiment, mice were terminally anaesthetized by a subcutaneous injection of a cocktail contain ketamine (100 mg/kg), atropine (50 μg/mL), and xylazine (10 mg/kg). Mice were bled by retro-orbital bleeding, and tissues were harvested after *in situ* perfusion with PBS. One mouse was excluded from the experiment due to presence of tumors.

Patient population

Human atherosclerotic plaques (n=9-15) and paired blood samples were obtained from 1 (age-associated B-cells; ABCs) or 6 (Gzmk^{+}CD8^{+} T-cells) female and 8 (age-associated B-cells; ABCs) or 9 (Gzmk^{+}CD8^{+} T-cells) male patients undergoing a carotid endarterectomy procedure at the Haaglanden Medical Center, location Westeinde (The Hague, The Netherlands). The study was approved by the Medical Ethical Committee of the HMC (NL71516.058.19). The study was performed in accordance with the declaration of Helsinki and all patients gave written informed consent at the start of the study.

Serum cholesterol, triglyceride and immunoglobulin measurements

Orbital blood was collected following euthanasia. Blood samples were centrifuged at high-speed (10,000 rpm) and serum was collected and frozen at -80 °C until further use. To determine total cholesterol levels and triglyceride levels, serum samples underwent enzymatic colorimetric procedures (Roche/Hitachi, Mannheim Germany) with precipath (Roche/Hitachi) as an internal standard. Total serum titers of IgM and oxLDL-specific IgM were measured by ELISA as previously described.[11]

Histology

Hearts and aortas were embedded in O.C.T. compound (Sakura) and snap-frozen. To determine lesion size, cryosections (10 μm) of the aortic root were stained with Oil-Red-O and hematoxylin (Sigma-Aldrich). To quantify lesion volume, sections were collected from when aortic valves started to appear. The average of five sequential sections of the three-valve area of aortic roots, displaying the highest lesion content, were used to compare the lesion size (mm^2). Collagen content in the lesions was quantified using a Masson's trichrome staining (Sigma-Aldrich). The necrotic core was defined as the acellular, debris-rich lesion area as percentage of total plaque area. Corresponding sections on separate slides were stained for monocyte/macrophage content with a MOMA-2 antibody (1:1000, AbD Serotec) followed by a biotinylated goat anti-rat IgG antibody (1:200, Vector). Secondary antibodies were detected using the Vectastain ABC kit (Vector) and visualized with ImmPACT NovaRED HRP substrate (Vector). We categorized cholesterol crystallization of atherosclerotic lesions in the aortic root on a scale of 0 (no cholesterol crystallization) to 3 (>75% of the lesion area contains crystalline cholesterol). Presence of calcification was manually scored based on morphology. Analysis and scoring were performed blinded. Mice with bicuspid aortic valves were excluded from histological analyses (n=3). Pictures were taken with a Mikrocam II (Besser) linked to a Leica DM6000 Microscope. Stained sections were manually analysed with ImageJ software.

Human tissue processing

Single cell suspensions of human carotid plaques were obtained as previously described.[12] Briefly, isolated plaques were digested using a mixture of RPMI 1640 containing 2.5 mg/mL Collagenase IV (ThermoFisher Scientific), 0.25 mg/mL DNAse I (Sigma), 2.5 mg/mL Albumin from Human Serum (Sigma-Aldrich) at 37°C for 30 minutes, and filtered through a 70 μm cell strainer (Major Resources Table in the Supplemental Materials). PBMCs were isolated by diluting whole blood 1:2 in PBS containing 2% heat-inactivated Fetal Bovine Serum (FBS), followed by a density gradient using SepMate™ PBMC isolation tubes (STEMCELL Technologies) containing Ficoll-Paque Premium™ (GE Healthcare). Subsequently, cells were centrifuged at 1200xg for 10 minutes at room temperature. PBMCs were isolated from the intermediate layer and washed twice with PBS + 2% FBS (250xg, 10 minutes, room temperature).

Flow cytometry

Immunostaining was performed as previously described on single cell suspensions derived from murine blood, spleen, and aortas,[13] and human PBMCs and plaques to characterize immune cells. Atherosclerotic aortic arches, from which perivascular adipose tissue was removed, were digested by incubation with a digestion mix (collagenase I 450 U/mL, collagenase XI 250 U/mL, DNAse 120 U/mL, and hyaluronidase 120 U/mL; all Sigma–Aldrich) for 30 min at 37°C while shaking, and subsequently strained over a 70 μm strainer. To block Fc receptors, an

unconjugated anti-CD16/32 antibody (clone 2.4G2, BD Bioscience) was used for mouse samples and Human TruStain FcX™ (Biolegend) for human samples. Living cells were selected using Fixable Viability Dye eFluor™ 780 (1:2000, eBioscience) and different cell populations were defined using anti-mouse and anti-human fluorochrome-conjugated antibodies (Major Resources Table in the Supplemental Materials). Antibody staining of transcription factors and cytokines was performed using transcription factor fixation/permeabilization concentrate and diluent solutions and cytofix/permeabilization solutions, respectively (BD Biosciences). FACS analysis was performed on a Cytoflex S (Beckman Coulter) and the acquired data were analyzed using FlowJo software.

Aortic CD45$^+$ cell isolation for single-cell RNA-sequencing

Atherosclerotic aortic arches, from which perivascular adipose tissue was removed, were isolated from young WD-fed (young WD) *Ldlr*$^{-/-}$ mice (4-5 months old; n=29) and old CD-fed (old CD) *Ldlr*$^{-/-}$ mice (22 months old; n=12) and enzymatically digested as described above. Single cell suspensions were stained with Fixable Viability Dye eFluor™ 780 (1:2000, eBioscience) and CD45-PE (1:500, clone 30-F11, Biolegend). After removing doublets, alive CD45$^+$ cells were sorted (Supplementary material Figure S1a) using a 100µm nozzle in PBS supplemented with 0.04% BSA using a FACS Aria II SORP (BD Biosciences) and immediately processed for single-cell RNA-sequencing (scRNA-seq).

Single-cell library preparation

Aortic CD45$^+$ cell suspensions were loaded on a Chromium Single Cell instrument (10x Genomics) to generate single cell gel bead emulsions (GEMs). ScRNA-seq libraries were prepared using the Single Cell 3$^{'}$ Solution v2 Reagent Kit (10xGenomics). Sequencing was performed on an Illumina HiSeq2500 and the digital expression matrix was generated by de-multiplexing barcode processing and gene UMI (unique molecular index) counting using the Cell Ranger v3.0 (aged) and v6.0 (young) pipeline (10x Genomics). Data quality is provided in Supplementary material Figure S1b-d.

Single-cell data processing and integrative analysis

The digital expression matrices were analyzed using Seurat, an R package designed for single cell RNA sequencing. Cells of young WD and old CD mice were filtered by unique gene count per cell >200 and <6800 for young WD; >200 and <7500 for old CD. In addition a cutoff was set to a maximum of 10% and 12% mitochondrial gene expression for young and aged samples, respectively (Supplementary material Figure S1c). Thereafter, data were log-normalized and gene expression was scaled. Using the DoubletDecon approach[14], 800 and 1237 counts were identified as doublets in the young WD and old CD set, respectively, and removed. Single-cell transcriptomes of CD45$^+$ cells isolated from aortas of young non-atherosclerotic chow diet-fed

Ldlr$^{-/-}$ mice (2 months old, n=9; GSM2882368)[9] were loaded and filtered from doublets and low quality cells by unique gene count per cell >500 and <3600 and a cutoff was set to a maximum of 5% mitochondrial gene expression.

Next, transcriptomes of the three datasets were integrated to perform comparative analysis on the remaining 372 (young CD), 4319 (young WD) and 4674 (old CD) cell counts. To reduce the dimensionality of the scaled data and create a cell clustering, principal component analysis (PCA) was performed, of which 12 PCA components were included for cluster detection at a resolution of 0.35 and subsequently visualized through Uniform Manifold Approximation and Projection (UMAP). The Seurat function FindAllMarkers was used to find the differentially expressed genes (DEGs) per cluster, which were examined to define the cell clusters. For the high-resolution re-clustering, (*Cd79b*$^{+}$) B-cell clusters, (*Cd3e*$^{+}$) T-cell clusters and (*Cd68*$^{+}$ and *Itgam*$^{+}$) myeloid clusters were selected and extracted from the main clustering. Thresholds were set to *Cd19*<0.3, *Cd79a*<0.3, *Cd79b*<0.3, *Cd68*<0.3 to exclude non-T-cells from the T-cell clustering, *Cd3e*<0.3, *Cd68*<0.3 to exclude non-B-cells from the B-cell clustering and *Cd3e*<0.3, *Cd19*<0.3, *Cd79b*<0.3 to exclude non-myeloid cells from the myeloid clustering. The variable genes of these selected clusters were then used as input for dimensionality reduction and re-clustering. PCA analysis on rescaled transcripts was performed with the following dimensions and resolutions: T-cells (3561 cells), dimensions 19, resolution 0.505; B-cells (2269 cells), dimensions 16, resolution 0.31; myeloid cells (1166 cells), dimensions 18, resolution 0.66. UMAP plots, dot plots, violin plots, volcano plots and heatmaps were generated in R. For comparison of Gzmk^{+} CD8^{+} T-cells with other CD8^{+} T-cells, a threshold was set to *Cd3e*>0.3, *Cd8a*>0.3, *Cd8b1*>0.3, *Cd4*<0.3, *Tcrg-C1*<0.3, and *Trdc*<0.3, followed by subsetting of CD8 clusters 2, 3, 5 and 6. Within cluster 2 of the B-cell clustering, bonafide age-associated B-cells (ABCs) were separated from plasma cells (PCs) by setting a threshold on *Igkc* expression levels: ABCs, *Igkc*<6.3 and PCs, *Igkc*>6.3 (Supplementary material Figure S6b). Differential gene expression of bonafide ABCs was used for volcano plot generation and pathway analysis in Figure 4. Clustered heatmaps showing the top 25 variable genes were produced in R with the pheatmap package. Pathway analysis was performed using Ingenuine Pathway Analysis (IPA) Software (Qiagen).

Projection of scRNA-seq analysis of aortic cells of non-atherosclerotic C57BL/6 mice onto *Ldlr*$^{-/-}$ aortas

Single-cell reference mapping was performed according the vignette "Mapping and annotating query datasets" (https://satijalab.org/seurat/articles/integration_mapping.html). Briefly, scRNA-seq data of C57BL/6 mice of 3-24 months of age[15], were loaded and excluded of non-immune cells (e.g. endothelial cells) by setting a threshold to *Ptprc*>0.3 & *Cdh5*<0.3 & *Cd34*<0.3 (Supplementary material Figure S6a). A total of 45 (3 months), 27 (18 months), and 9 (24 months) aortic immune cells were included in this analysis and set as query dataset. Our

scRNA-seq dataset of atherosclerotic aortas from *Ldlr*$^{-/-}$ mice was set as reference dataset. The TransferData function was used to predict the cell type of the query cells according the *Ldlr*$^{-/-}$ clustering. With the MapQuery function, the query cells were projected onto the *Ldlr*$^{-/-}$ UMAP structure.

PMA/ionomycin stimulation

Cells were cultured at 37 °C, 5% CO_2 in complete medium (RPMI 1640 containing 5% heat-inactivated FBS, L-glutamine, 100 IU/ml penicillin, 100 µg/ml streptomycin and 0.05 mM β-mercaptoethanol). Single cell suspensions from the spleen were stimulated for 4 hours with PMA (50 ng/ml, Sigma), ionomycin (500 ng/ml, Sigma) and the Golgi-plug brefeldin A (3 µg/ml, Thermofisher). Intracellular cytokine expression was measured using flow cytometry.

In vitro antigen presentation assay

Splenic CD19$^+$CD21$^-$CD23$^-$CD11b$^+$/CD11c$^+$ ABCs and CD19$^+$CD21$^+$CD23$^+$ follicular (FO) B-cells from aged female *Ldlr*$^{-/-}$ mice (aged 12-20 months old, n=5) were isolated with flow sorting (Supplementary material Figure S6c). ABCs or FO B-cells were exposed to OVA323 peptide antigen or control medium for 4 hours at 37ºC 5% CO2. The B-cells were washed to remove excessive OVA323 and subsequently co-cultured in a 1:1 ratio with CD4$^+$ T-cells from OTII mice for 24 hours, after which activated CD69$^+$ cells were measured as percentage CD4$^+$ T-cells with flow cytometry. Proliferation was assessed by co-culturing OVA323-exposed B-cells with CFSE-labeled CD4$^+$ T-cells for 72 hours, followed by measurement of CFSE dilution.

Macrophage polarization and in vitro phagocytosis assay

Bone marrow cells were isolated from young and aged chow diet-fed *Ldlr*$^{-/-}$ mice (n=5 per group) and cultured into bone marrow-derived macrophages (BMDMs) with 20 ng/ml M-CSF. BMDMs were polarized towards an M1-like (stimulated with 100 ng/ml LPS and 100 ng/ml IFN-g) or M2-like (stimulated with 20 ng/ml IL-4 and 20 ng/ml IL-13) phenotype. To assess efferocytosis capacity, M1 and M2 macrophages were exposed to CFSE-labeled apoptotic splenocytes (made apoptotic by incubating splenocytes with 1% Brefeldin A for 24h) for 2h, after which uptake was measured by flow cytometry. To assess lipid uptake, macrophages were cultured with 4 µM cholesteryl-BODIPY FL C_{12} (Invitrogen, #C3927MP) for 24h, followed by measurement of alive BODIPY$^+$ (lipid-laden) macrophages using flow cytometry.

Statistical analysis

Data are expressed as mean ± SEM. Outliers were identified and removed using Grubbs outlier tests (α = 0.05). Significance of mouse data with 3 groups was tested using an ordinary one-way ANOVA test or nonparametric Kruskal-Wallis test followed by a Tukey or Dunn multiple comparisons test, respectively. Significance of young versus aged BMDMs was tested by two-tailed unpaired t-test. Significance of follicular B-cells versus age-associated B-cells was tested

by two-tailed paired t-test. Significance of human data was tested using a two-tailed paired t-test. P-values of <0.05 were considered significant. Statistical analysis was performed using GraphPad Prism 9.0.

Data availability

In silico data analysis was performed using custom R scripts (R version 4.1.2) designed especially for this research and/or based on the recommended pipelines from the pre-existing packages listed in the individual segments above. Single-cell RNA sequencing data are available upon personal request from the corresponding author (a.c.foks@lacdr.leidenuniv.nl)

SUPPLEMENTARY FIGURES

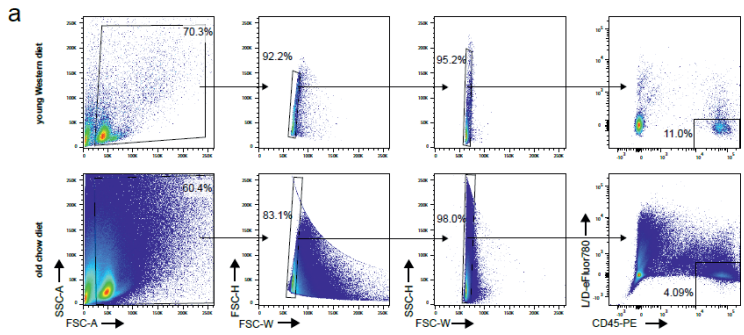

b

Metrics aortic CD45⁺ cells	young Western diet	old chow diet
Estimated Number of Cells	5,286	6,430
Mean Reads per Cell	40,159	98,316
Median Genes per Cell	1,816	4,518
Number of Reads	21,227,807	632,170,175
Total Genes Detected	19,393	38,109
Median UMI Counts per Cell	5,021	7,238
Valid Barcodes	97.0%	98.3%
Sequencing Saturation	57.1%	76.5%
Q30 Bases in Barcode	93.5%	97.2%
Q30 Bases in RNA Read	87.5%	67.1%
Q30 Bases in UMI	89.9%	97.1%
Reads Mapped to Genome	92.9%	86.7%
Reads Mapped Confidently to Genome	90.4%	83.7%
Reads Mapped Confidently to Intergenic Regions	4.3%	3.6%
Reads Mapped Confidently to Intronic Regions	30.7%	22.4%
Reads Mapped Confidently to Exonic Regions	55.3%	57.8%
Reads Mapped Confidently to Transcriptome	50.4%	55.2%
Reads Mapped Antisense to Gene	2.5%	0.9%
Fraction Reads in Cells	93.9%	91.4%

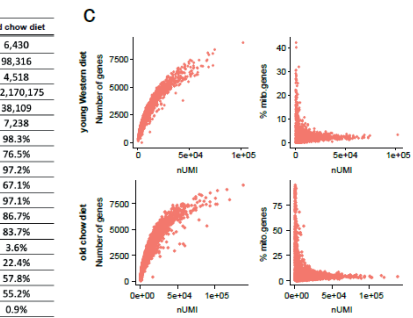

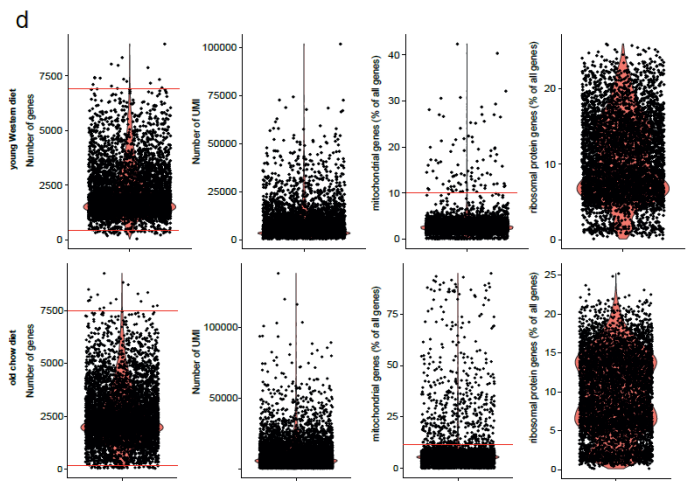

Supplementary Figure 1. Gating strategy of aortic CD45⁺ cells and quality control for single-cell RNA sequencing of aortic CD45⁺ cells.

a, Gating strategy of alive aortic CD45⁺ cells from Western-diet fed young (young WD) and chow diet-fed aged (old CD) *Ldlr*$^{-/-}$ mice. **b**, Sequencing parameters from single cell CD45⁺ suspensions loaded on the 10xGenomics Chromium scRNA-seq platform. **c**, Plots showing number genes and percentage of mitochondrial genes (% mito.genes) in relation to UMI counts. **d**, Number of genes and unique molecular identifier (UMI), and percentage of mitochondrial genes and ribosomal proteins (expressed as % of all genes) in the single cells. Cells with gene number between 200-6800 (young WD) or 200-7500 (old CD) were included (indicated by red lines). A cutoff was set to 10% (young WD) or 12% (old CD) mitochondrial genes (indicated by red lines).

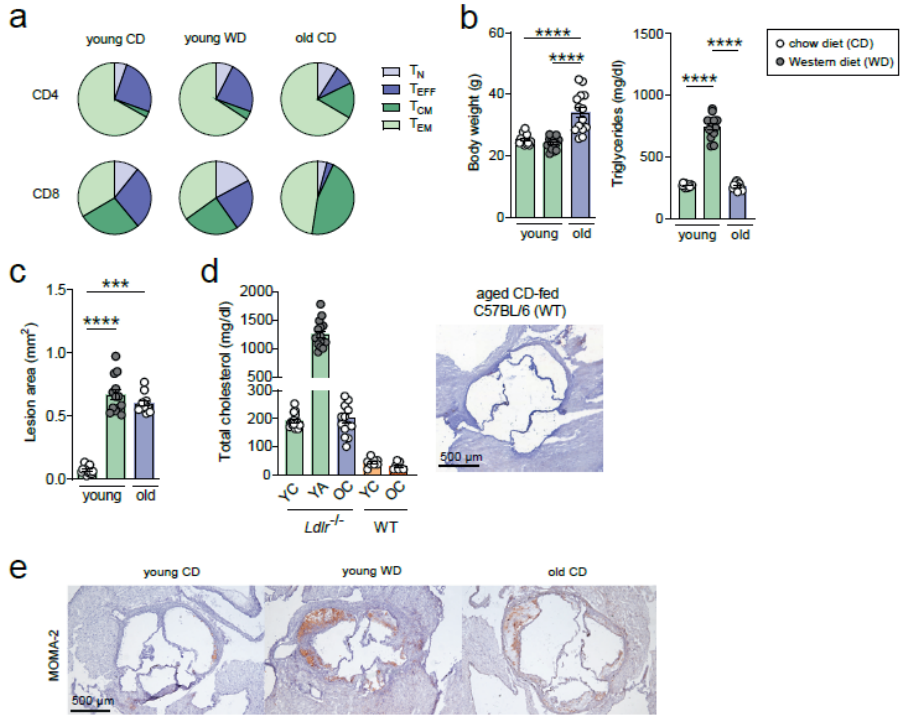

Supplementary Figure 2. Shift from naïve to memory T-cells in spleens of aged *Ldlr*$^{-/-}$ mice.
Ldlr$^{-/-}$ mice aged 3 months (green bars) or 20 months (violet bars) were fed a standard chow diet (white circles) or a western-type diet (grey circles) for 10 weeks. **a**, Circulating naïve (T_N: $CD44^-CD62L^+$), effector (T_{EFF}: $CD44^-CD62L^-$), central memory (T_{CM}: $CD44^+CD62L^+$) T-cells, and effector memory (T_{EM}: $CD44^+CD62L^-$) were measured and quantified as a percentage of $CD4^+$ and $CD8^+$ T-cells and plotted in a pie chart. **b**, Body weight and triglyceride levels at sacrifice were measured. **c,** Cross sections of the aortic root were stained with Oil-Red-O for lipid content and atherosclerotic lesion area was quantified. **d**, Total serum cholesterol levels of young and aged *Ldlr*$^{-/-}$ and wildtype C57BL6 (WT) mice at sacrifice and representative picture of Oil-Red-O stained cross section of the aortic root of a 20-month old C57BL/6 mouse. **e,** Representative pictures of MOMA-2 stained cryosections of the aortic root. Data are from n=8–15 mice per group. Statistical significance was tested by one-way ANOVA. Mean ± SEM plotted. ***P<0.001, ****P<0.0001.

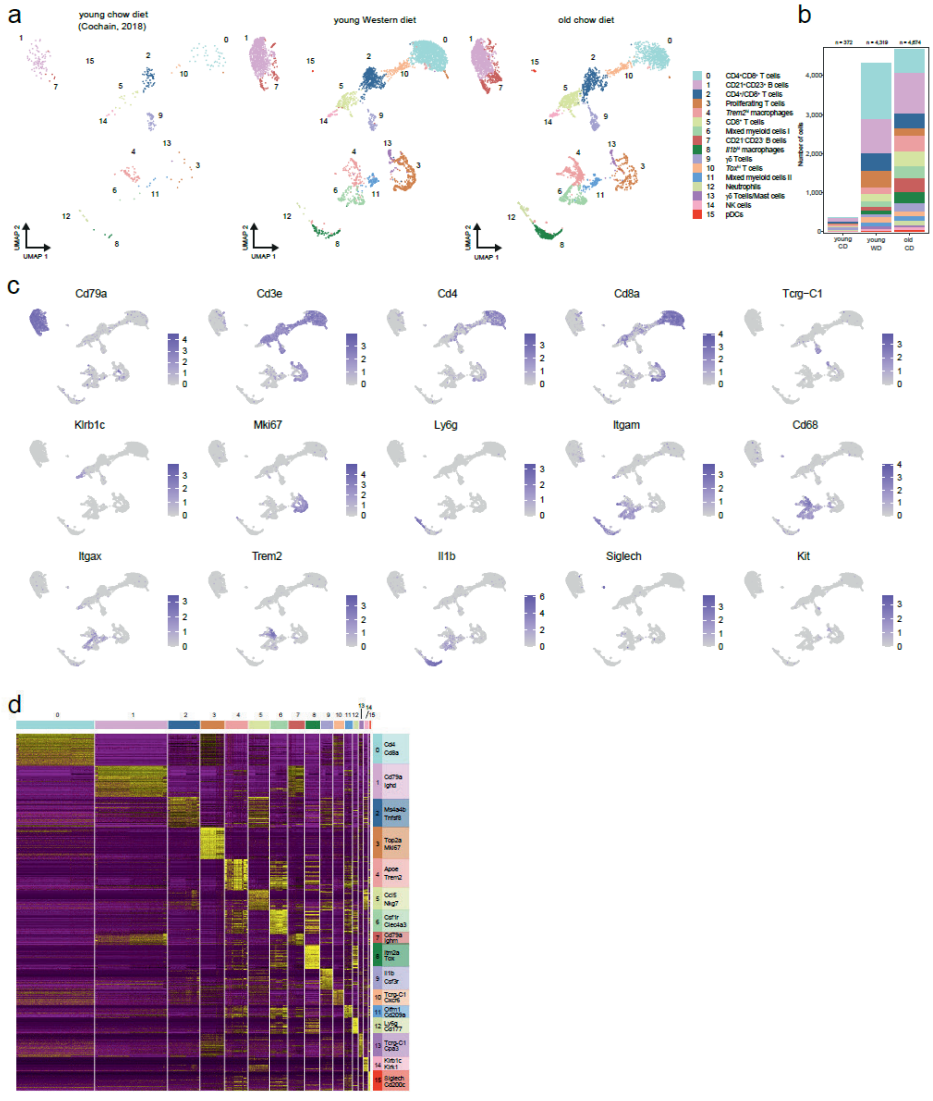

Supplementary Figure 3. Single-cell RNA sequencing on aortic leukocytes of *Ldlr*$^{-/-}$ mice.
a, UMAP plots and **b,** stacked diagrams of absolute cell counts of identified immune cell clusters in young CD, young WD and old CD aortas. **c**, Average expression of immune cell lineage markers mapped onto the UMAP plot. **d,** Heatmap of the top 50 differentially expressed genes (normalized single-cell gene expression shown) per cluster and selected enriched genes used for identity annotation of cell clusters in Figure 2c and Supplementary material Figure S3a.

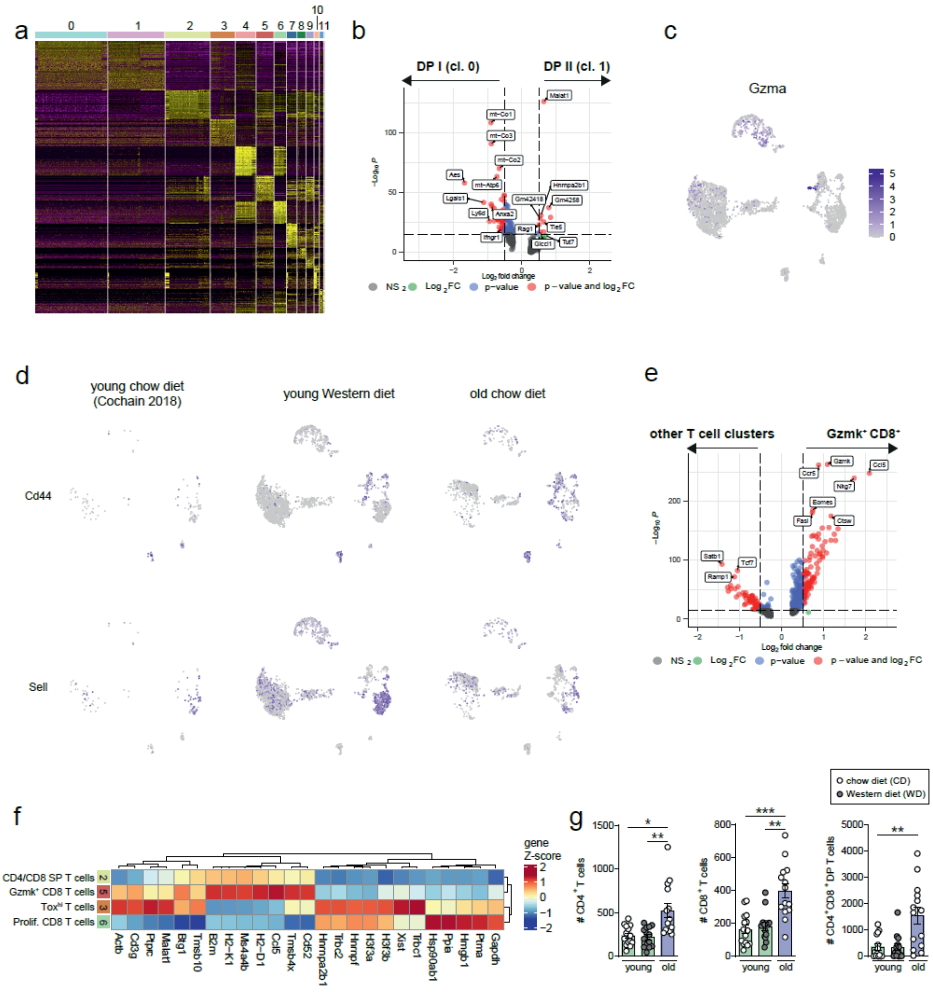

Supplementary Figure 4. Expression of T-cell-related markers in T-cell clustering.

Cd3e^{+} clusters were extracted from the principal clustering and reclustered. **a**, Heatmap of the top 50 differentially expressed genes per cluster (normalized single-cell gene expression shown). **b**, Volcano plot of the differentially expressed genes (DEGs) in the CD4^{+}CD8^{+} double positive (DP) I (cluster 0) compared to DP II (cluster 1) T-cell cluster. **c**, Feature plots show relative gene expression of *Gzma* (Granzyme A), **d**, *Cd44* and *Sell* (CD62L) within the T-cell subclustering. **e**, Volcano plot of the differentially expressed genes (DEGs) in the Gzmk^{+}CD8^{+} T-cell cluster compared to other T-cell clusters. **f**, Heatmap of hierarchically clustered top 25 variable genes across CD8^{+} T-cells in cluster 2, 3, 5 and 6. **g,** Using flow cytometry, absolute numbers of CD4^{+} T-cells, CD8^{+} T-cells, and CD4^{+}CD8^{+} DP T-cells were measured in aortas of young and aged *Ldlr*$^{-/-}$ mice (n=12-15). Gating strategy is shown in Supplementary material Figure S5a. Statistical significance was tested by one-way ANOVA. Mean ± SEM plotted. *P<0.05, **P<0.01, ***P<0.001. DP: double positive, SP: single positive.

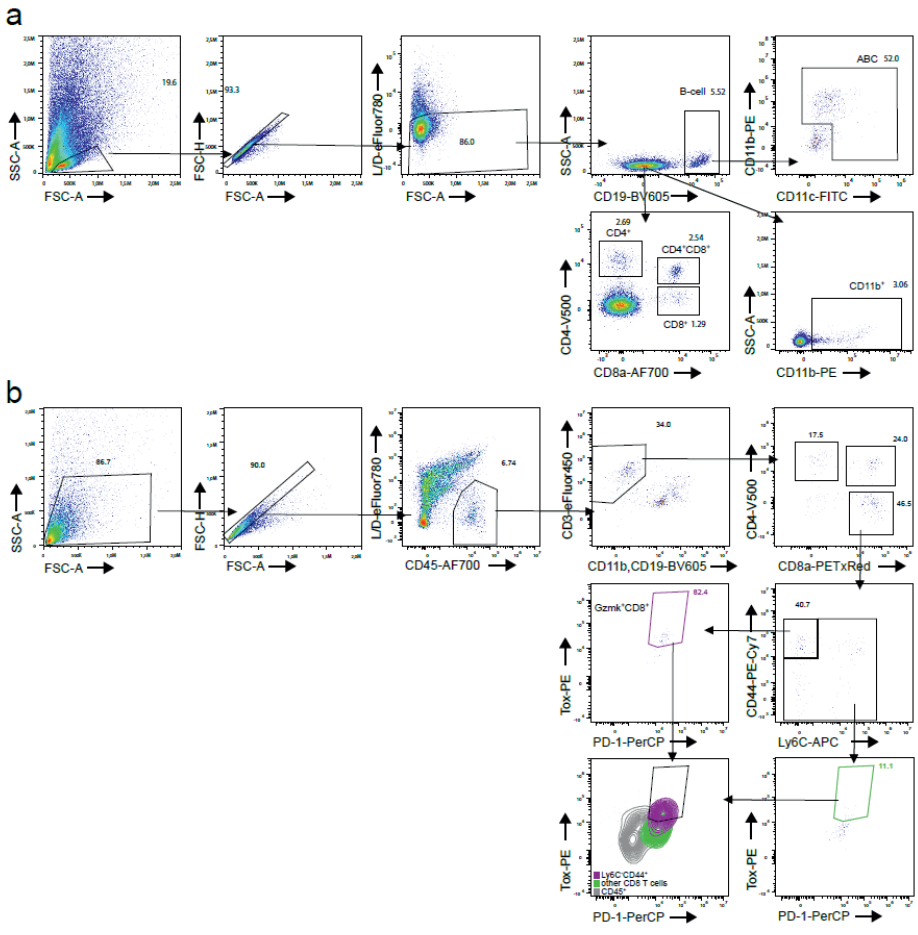

Supplementary Figure 5. Gating strategy of immune cell populations in aged aorta.

a, Gating strategy of aortic CD19$^+$ B-cells, CD11b$^+$ and/or CD11c$^+$ age-associated B-cells, CD11b$^+$ myeloid cells, CD4$^+$, CD8$^+$ and CD4$^+$CD8$^+$ T-cells, and of **b**, Ly6C$^-$CD44$^+$Tox$^+$PD-1$^+$ CD8$^+$ T-cells (GzmK$^+$ CD8 T-cells) aortic cells from *Ldlr*$^{-/-}$ mice.

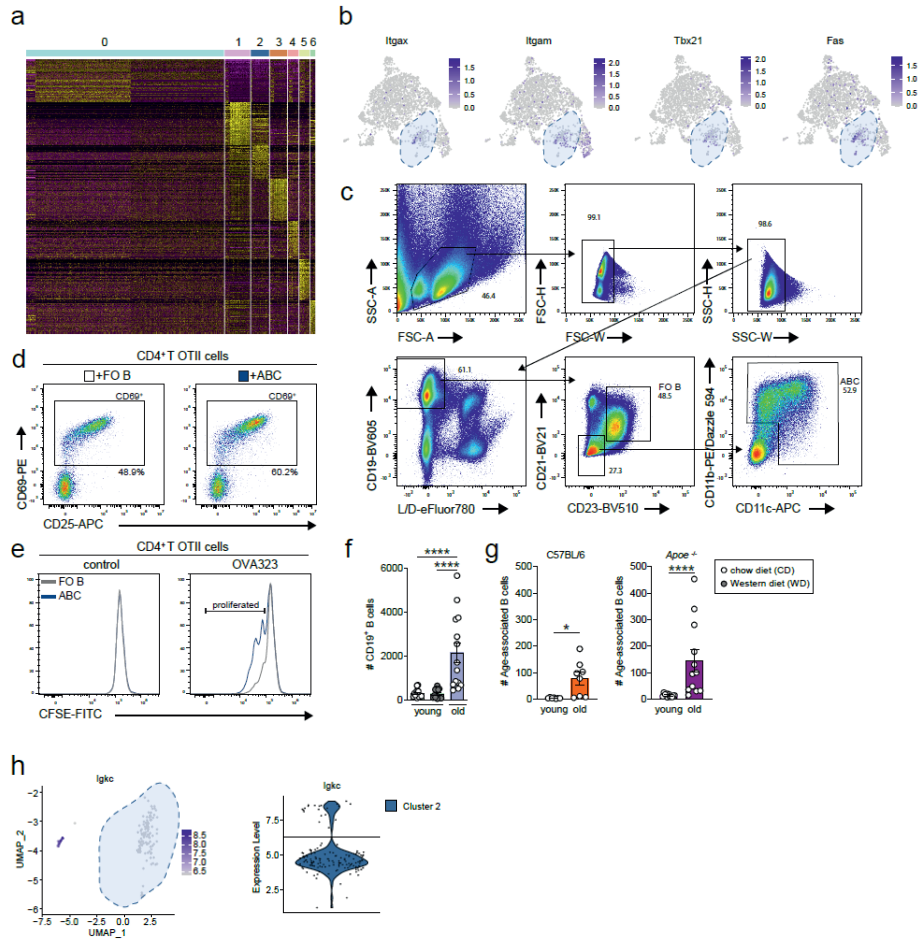

Supplementary Figure 6. Age-associated B-cell markers, antigen presentation capacity and abundance in aortas of atherosclerotic and wildtype C57BL/6 mice.

Cd79a^{+} clusters were extracted from the principal clustering and reclustered. **a**, Heatmap of the top 50 differentially expressed genes per cluster (normalized single-cell gene expression shown). **b**, Average expression of age-associated B-cell (ABC) markers *Itgam* (CD11b), *Itgax* (CD11c), *Tbx21* (T-bet) and *Fas* was mapped onto the UMAP plot, in which ABCs are encircled in the dashed blue shape. **c**, Gating scheme for flow sorting of splenic CD19^{+}CD21^{-}CD23^{-}CD11b^{+}/CD11c^{+} ABCs and CD19^{+}CD21^{+}CD23^{+} follicular (FO) B-cells from aged female *Ldlr*$^{-/-}$ mice. **d**, Representative flow cytometry plots of CD69^{+} activation or **e**, proliferation in CD4^{+} OTII T-cells after presentation of OVA323 antigen by ABCs and follicular (FO) B-cells. **f**, Using flow cytometry, absolute numbers of CD19^{+} B-cells were measured in aortas of young and aged *Ldlr*$^{-/-}$ mice (n=12-15). **g**, Absolute numbers of ABCs in aortas of young and aged C57BL/6 and *Apoe*$^{-/-}$ mice were determined with flow cytometry. Mouse data are from n=8–15 mice per group. Gating strategy is shown in Supplementary material Figure S5a. **h**, Expression plots of cluster 2 (ABCs/plasma cells) showing differential expression levels of *Igkc*, that encodes for the constant region of the kappa chain in immunoglobulins, in ABCs (*Igkc* < 6.3) and plasma cells (*Igkc* > 6.3). Statistical significance was tested by one-way ANOVA (3 groups) or two-tailed unpaired t-test (2 groups). Mean ± SEM plotted. *P<0.05, ****P<0.0001.

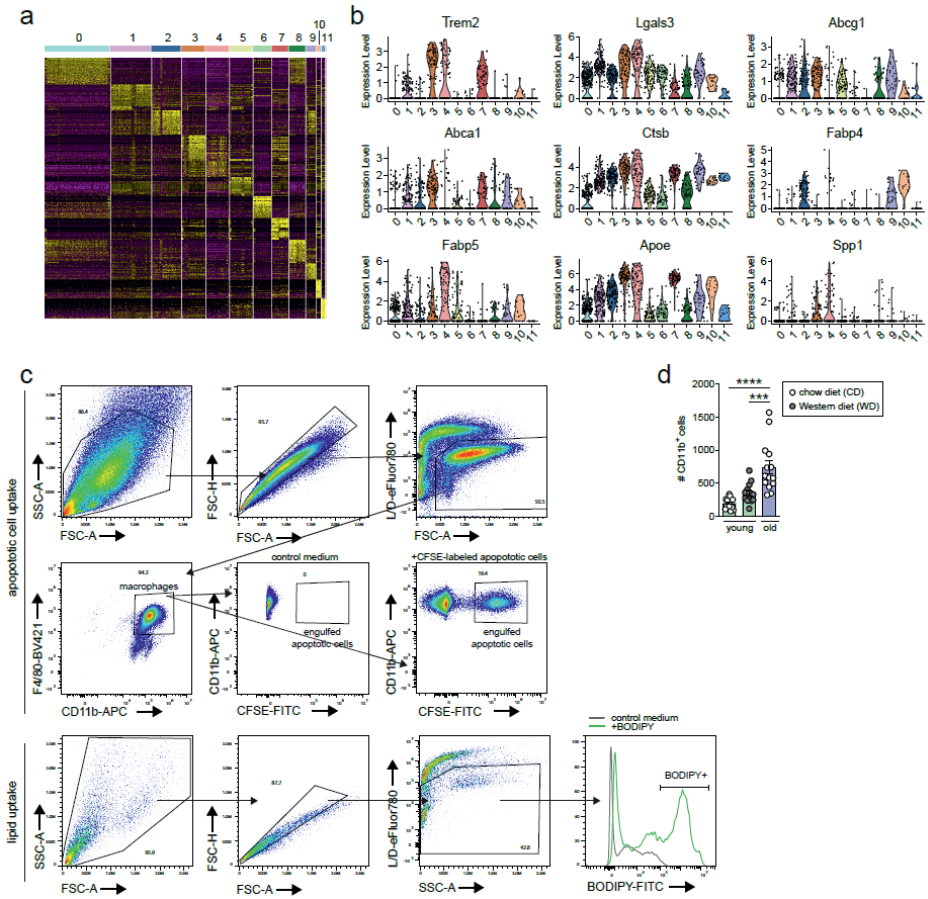

Supplementary Figure 7. Expression of myeloid cell markers and macrophage phagocytosis gating strategy.
Cd68^{+} and *Itgam*$^{+}$ clusters were extracted from the principal clustering and reclustered. **a**, Heatmap of the top 50 differentially expressed genes per cluster (normalized single-cell gene expression shown). **b**, Violin plots showing the average expression of foamy macrophage markers. **c**, Gating strategy of bone marrow-derived macrophages that have taken up CFSE-labeled apoptotic cells (upper) or BODIPY-labeled cholesteryl (lower). d, Using flow cytometry, absolute numbers of CD11b^{+} myeloid cells were measured in aortas of young and aged *Ldlr*$^{-/-}$ mice (n=12-15), of which the gating strategy is shown in Supplementary material Figure S5a. Statistical significance was tested by one-way ANOVA. Mean ± SEM plotted. ***P<0.001, ****P<0.0001.

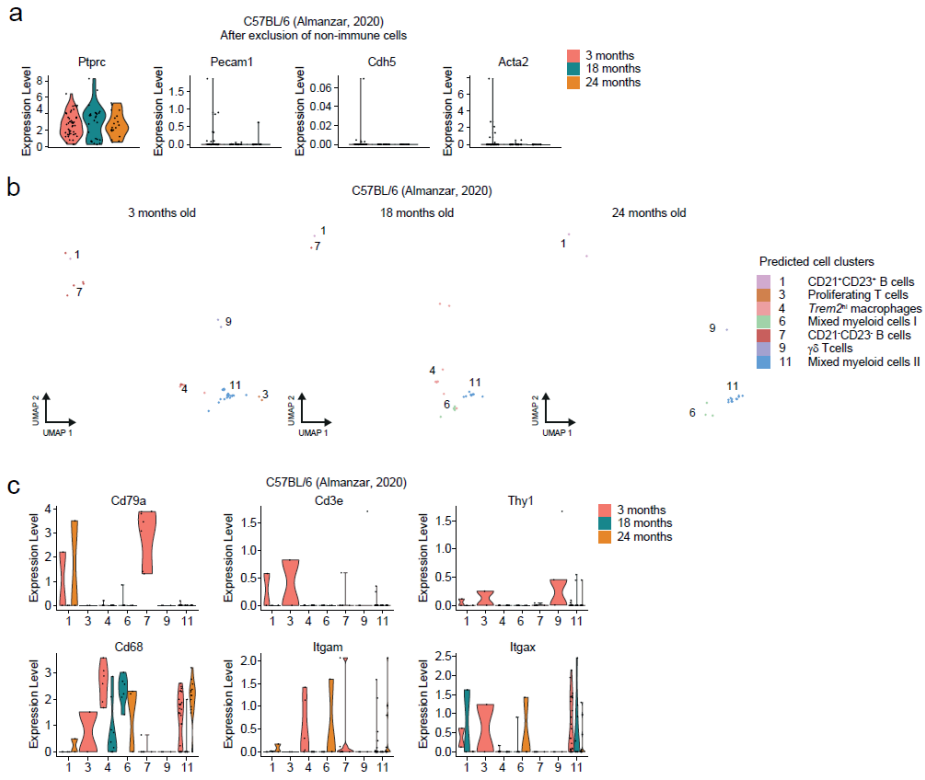

Supplementary Figure 8. Projected single-cell transcriptomes of leukocytes from non-atherosclerotic C57BL6 mice aortas onto atherosclerotic aortas of *Ldlr*$^{-/-}$ mice.

a, Violin plots depicting the average expression of immune cell and endothelial markers after excluding non-immune cells in aortic cells of C57BL/6 mice. **b,** Projection of aortic cells from young (3 months, n=11) and aged (18 months, n=6 and 24 months, n=4) C57BL/6 mice on the reference set. **c,** Violin plots depicting the average expression of canonical immune cell markers in predicted clusters of aortic cells from C57BL/6 mice.

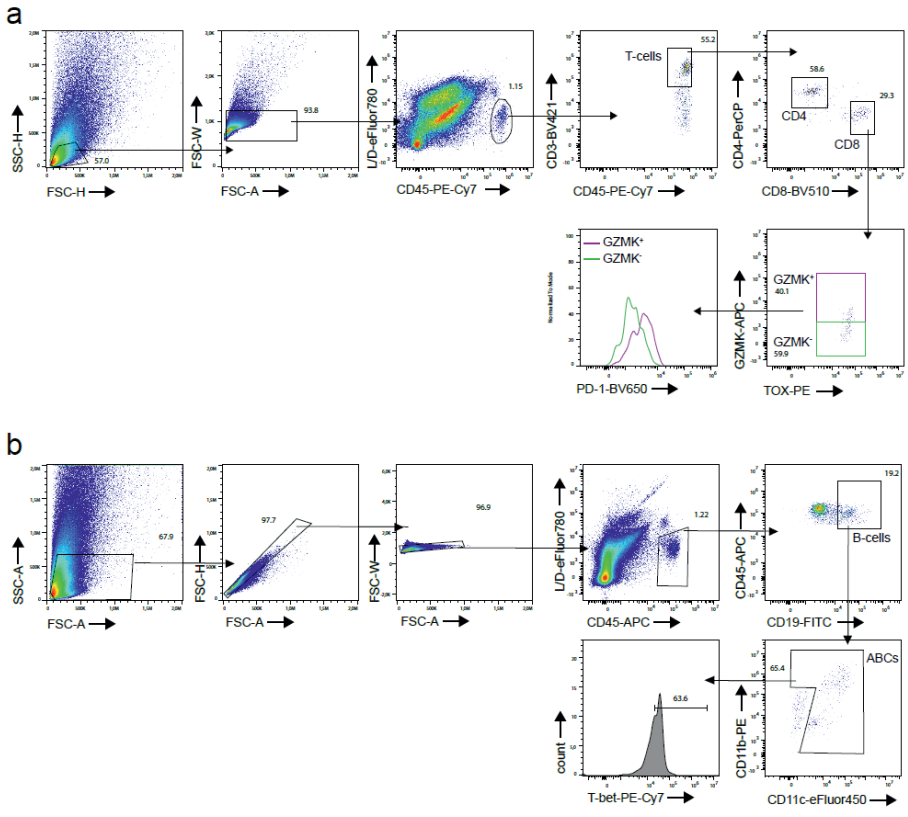

Supplementary Figure 9. Gating strategy of age-associated T- and B-cells in human atherosclerotic plaques.
Gating strategy of **a**, GZMK^{+}TOX^{+}CD8^{+} T-cells and **b,** CD19^{+} CD11b^{+} and/or CD11c^{+} age-associated B-cells and T-bet within age-associated B-cells in human carotid atherosclerotic plaques.

SUPPLEMENTARY TABLES

Supplementary Table 1. Main Clustering top 20 differentially expressed genes

Main.00	Main.01	Main.02	Main.03	Main.04	Main.05	Main.06	Main.07
$CD4^+CD8^+$ DP T cells	**$CD21^+CD23^+$ B cells**	**$CD4^+$/$CD8^+$ T cells**	**Prolif. T cells**	**$Trem2^{hi}$ MF**	**$CD8^+$ T cells**	**Mixed myeloid cells I**	**$CD21^-$ $CD23^-$ B cells**
Rag1	Cd79a	Ms4a4b	Mki67	C1qa	Ccl5	Ifitm3	Mzb1
Arpp21	Ebf1	Ms4a6b	Top2a	C1qb	Nkg7	Ms4a6c	Ms4a1
Cd8b1	Cd79b	Il7r	Pclaf	C1qc	Ms4a4b	Fcer1g	Iglc2
Ccr9	Ighd	Gm2682	Stmn1	Cd63	Ctsw	Cebpb	Iglc1
Dntt	Ms4a1	Dapl1	Hist1h2ae	Fcer1g	AW112010	Lst1	Iglc3
Cd8a	Iglc2	Igfbp4	Hist1h1b	Lgmn	Ctla2a	Csf1r	Pkig
Themis	Fcmr	Inpp4b	Hist1h2ap	Ms4a7	Il2rb	Cybb	Cd79a
Gm4258	H2-Aa	S1pr1	Hist1h3c	Cd68	Cxcr6	Mpeg1	H2-DMb2
Endou	Mef2c	Ccnd2	Birc5	Pf4	Klrd1	Clec4a3	Ly6a
Ldhb	H2-Eb1	Lef1	Hist1h2ab	Trf	Klrk1	Ifitm2	Ebf1
Rmnd5a	Bank1	Gimap3	Ube2c	Mafb	Cxcr3	Cx3cr1	Igkc
Cd4	Iglc3	Atp1b3	Rrm2	Wfdc17	Gzmk	Hp	Bank1
Sox4	Cd74	Ccr7	Cenpf	Csf1r	Hcst	Clec4a1	Napsa
Ssbp2	Igkc	Smad7	Hmgn2	Fcgr3	Gimap4	Ifitm6	Cd79b
Tcf7	H2-DMb2	Chd3	Dut	Mt1	H2-Q7	Ear2	Ighm
Satb1	H2-Ab1	Gm12840	Nusap1	Ctsb	Ms4a6b	Lgals3	H2-Eb1
Myb	H2-Ob	Hcst	Tuba1b	Apoe	Id2	S100a4	Cd74
Aqp11	Pax5	H2-Q7	Hmgb2	Tyrobp	Gimap3	Tyrobp	Plac8
Lck	Gm31243	Trac	Spc24	Lyz2	Ly6c2	Lyz2	H2-Ab1
Trbc2	Fcer2a	AW112010	Cdca8	Lgals3	S100a6	Gngt2	H2-Aa

Main.08	Main.09	Main.10	Main.11	Main.12	Main.13	Main.14	Main.15
$Il1b^{hi}$ MF	**gd T cells**	**Tox^{hi} T cells**	**Mixed myeloid cells II**	**Neutrophils**	**gd T cells/ MCs**	**NK cells**	**pDCs**
Il1b	Tmem176a	Tox	Olfm1	Ltf	Gm4632	Ncr1	Siglech
Retnlg	Cxcr6	Itm2a	Ccnd1	Wfdc21	Adgrg1	Klrk1	Cox6a2
Csf3r	Tmem176b	Cd5	Cd209a	Cd177	Myl10	Klre1	Gm21762
Slpi	Il7r	Lef1	Plbd1	Ly6g	Tcrg-C1	Klrb1c	Upb1
Cxcr2	Il18r1	Cd28	H2-DMb1	Chil3	Il2ra	Gzmb	Smim5
Mmp9	Rora	Trac	Ckb	Lcn2	Tcrg-C2	Klrc2	Ccnd1
Hdc	Actn2	Rgs10	Syngr2	Ngp	Tcrg-C4	Klra7	Runx2
Ifitm1	Ltb4r1	Ccr9	Ifitm2	Mmp8	Cdk6	Prf1	Lair1
Msrb1	Tcrg-C1	Sox4	S100a4	Mmp9	Hes1	Klrd1	Atp1b1
Hp	Podnl1	Satb1	Alox5ap	Ifitm6	Ptcra	Serpinb9	Mpeg1

Ccl6	S100a4	Cd2	Lgals3	Mgst1	Notch1	Il2rb	Ly6c2
Ifitm2	Tmem64	Cd27	Ifitm3	Camp	Uck2	Nkg7	Rnase6
Tnfaip2	Maf	Cd3d	Gm2a	Adpgk	Fkbp5	Gzma	Grn
Tyrobp	Ccr2	Ikzf2	H2-Ab1	Hp	Hdac4	Ctsw	Pld4
Grina	Ckb	Cd6	Cst3	Anxa1	Stmn1	Ccl5	Ctsl
Mxd1	Id2	Tespa1	H2-Aa	Retnlg	Myb	AW112010	Irf8
Ccr1	Itgb7	Trbc2	H2-Eb1	Pglyrp1	Plac8	Id2	Tcf4
S100a8	Cd82	Arap2	Tyrobp	S100a8	Sox4	Ms4a4b	Bst2
Cxcl2	Lmo4	Tcf7	Fcer1g	S100a9	Rgcc	Fcer1g	Plac8
S100a9	S100a6	Hivep3	Cd74	Lyz2	Dntt	Tyrobp	Tyrobp

Supplementary Table 2. T cell clustering top 20 differentially expressed genes

T.00	**T.01**	**T.02**	**T.03**	**T.04**	**T.05**	**T.06**	**T.07**
DP T cells I	**DP T cells II**	**$CD4^+$/$CD8^+$ T cells**	**Tox^{hi} T cells**	**Prolif. DP T cells**	**$Gzmk^+$ $CD8^+$ T cells**	**Prolif. $CD8^+$ T cells**	**$Il17a^+$ gd T cells**
Rag1	Cd8b1	S1pr1	Tox	Mki67	Gzmk	Cdc6	Serpinb1a
Arpp21	Dntt	Ccr7	Cd5	Top2a	Ccr5	Chek1	Pxdc1
Gm4258	Endou	Igfbp4	Itm2a	Hist1h3c	Ccl5	Cenps	Ly6g5b
Mier1	Cd8a	Klf2	Nab2	Birc5	Nkg7	Mcm10	Kcnk1
Themis	Arpp21	Ms4a4b	Rgs10	Pclaf	Eomes	Shmt1	Il1r1
Rmnd5a	Rag1	Smad7	Cd2	Ube2c	Fasl	Syce2	Il23r
Arl5c	Trbc2	Rps24	Cd28	Nusap1	Ctsw	Dhfr	Ltb4r1
Ccr9	Ldhb	Rps16	Lef1	Cenpf	Ctla2a	Exo1	Aqp3
Glcci1	Gmfg	Gm2682	B630019A10Rik	Cdca8	Gimap7	Ccne2	Actn2
Cd8b1	Lck	Rps7	Ikzf2	Kif11	AW112010	E2f1	Tmem176a
Satb1	Aqp11	Rps18	Tmsb10	Prc1	Ccl4	Hells	Fam83a
Lck	Cyb5a	Rps19	Hivep3	Knl1	Ms4a4b	Ncapg2	Blk
Ssbp2	Rmnd5a	Rps15a	Trac	Tpx2	Serpina3g	Chaf1a	Cpe
Cd4	Dgkeos	Rpl23	Actg1	Cenpe	Hopx	Aunip	Zbtb16
Ets2	Satb1	Rplp1	Rap1a	Ccnb2	Gzmb	Cdc45	Tmem176b
Cd8a	Chrna9	Rpl12	39326	Spc24	Il2rb	Rad51	Rbpms2
Ldhb	Mier1	Rpl17	Ccr4	Cdca3	H2-Q7	Gins1	Podnl1
Dntt	Ly6d	Rpl13	Arap2	Ccna2	S100a6	Nt5dc2	Ckb
Myb	Cd4	Rps20	Ikzf1	Cks1b	Rgs1	Fignl1	Rnase4
Cbl	Ccnd3	Rpl21	Cytip	Cdk1	Ahnak	Rrm2	Sdc1

T.08	**T.09**	**T.10**	**T.11**
Tregs	**NKT cells**	**MCs**	**gd T cells/ MCs**
Gpm6b	Klrb1c	Il1rl1	Nfe2

Tnfrsf4	Klra7	Arg1	Gm4632
Izumo1r	Styk1	Ccdc184	Gm5111
Foxp3	Klrc2	Hs3st1	Cd34
Tnfsf8	Klra9	Lpcat2	Gm12503
Ttn	Klre1	Dach2	Cpa3
Pou2f2	Klrk1	Slc7a8	Muc13
Nt5e	Xcl1	Rnf128	Epb41l4b
Ctla4	Ly6c2	Areg	Rab44
Maf	Klra6	Hba-a1	Gata2
Ifi27l2a	Klra1	Igsf5	Bcl11a
Eea1	Itga1	Rab27b	Paqr5
Syt11	Klrd1	Klrg1	Scin
Tbc1d4	Qrfp	Ptgir	Rgs18
Capg	Cd7	Pard3	Adgrg1
Ly6a	Pglyrp1	Ltb4r1	Gria3
Il2rb	Ctsw	Pparg	Adgrg3
Pear1	Il2rb	Gcnt1	Meis1
Sdcbp2	Klrc1	42248	Capn5
Icos	Nkg7	Nrgn	Cpne2

Supplementary Table 3. B cell clustering top 20 differentially expressed genes

B.00	B.01	B.02	B.03	B.04	B.05	B.06
B2 B cells	**B1/Bregs**	**ABCs/PCs**	**Activated B cells**	**Immature B cells**	**Ifn-induced B cells**	**Senescent B cells**
Ighd	Ahnak2	Dnm3	Mettl1	Akap12	Ifit3	Myadm
Fcer2a	1810046K07Rik	AC168977.1	Srm	Atp1b1	Ifit3b	Gm26532
Sell	Krt18	Nt5e	Eif4a1	Fam129c	Ifit1	Lmna
Mef2c	Zbtb32	Itm2c	Nme1	Cplx2	Usp18	Dyrk3
Ralgps2	Gnb3	AC133103.1	Hsp90ab1	Nedd4	Irf7	Ahnak
Cd55	Asph	C130026I21Rik	Ncl	Wfdc21	Rsad2	Tagln2
Neurl3	Gm30382	Itgb1	Ppp1r14b	Vpreb3	Slfn5	Ralgds
Fchsd2	Nid1	Lipc	Ranbp1	Cd93	Oasl1	Vim
Satb1	Ctla4	Havcr1	Mif	Sox4	Rtp4	Atrnl1
Stk17b	Krt222	Adgre1	Eif5a	Myb	Ifi206	Crip2
Ets1	Gm15228	Fas	Nop58	Ly6d	Zbp1	Atp2b1
Smad7	Dnase1l3	Fam46c	Apex1	Cd24a	Isg15	Cpm
Rpl13a	Csf2rb	Bhlhe41	Npm1	Spib	Oasl2	Cd2
H2-Ob	Tubb6	Spn	C1qbp	Coq7	Ifit2	Klf4
Cr2	Sox5	Fgl2	Ppa1	Serinc5	Ifi47	Adgre5
Gm31243	Nacc2	Ighg3	Ran	Myl4	Trim30a	Klf6

Lmo2	S100a6	Cacna1s	Fbl	4930426D05Rik	Ifi213	Pgap1
Pxk	Slamf9	Rgs10	Ddx21	Zeb2	Oas3	S100a6
Zfp318	Zfp811	Fah	Set	Chchd10	Ifi27l2a	Dennd4a
Pxdc1	Gas7	Tbx21	Bzw2	Pafah1b3	Ifi208	Rabgap1l

Supplementary Table 4. Myeloid cell clustering top 20 differentially expressed genes

My.00	My.01	My.02	My.03	My.04	My.05	My.06	My.07
M1 MFs	**Ccr2^{hi} Mono/MF**	**Nr4a1^{hi} Mono/MF**	**Trem2^{hi} MF**	**Foamy MF**	**Mono/MF/ DC**	**Neutrophils**	**Resident MF**
Cxcr2	Ccr2	Ace	Olfml3	Atp6v0d2	Flt3	Itgb2l	Cbr2
Csf3r	Fn1	Adgre4	Nes	Cd63	Klrd1	Ltf	Cd163
Retnlg	Ms4a4c	Eno3	Cadm1	Rplp1	Klrk1	4930438A08Rik	Lyve1
Mmp9	S100a4	Cd300e	Apbb2	Rpl38	Zbtb46	Abca13	Folr2
S100a11	Ifi211	Slc12a2	Tanc2	Ftl1	Olfm1	Cebpe	Gas6
Msrb1	Ly6c2	S1pr5	Ms4a14	C1qb	Dpp4	Mgst2	Mgl2
Slpi	F10	Spn	Ms4a7	Igf1	Ciita	Ly6g	Igfbp4
Hdc	Tmsb10	Treml4	Abcc3	Gpnmb	Kmo	Camp	Tmod1
Grina	Plac8	Pou2f2	Hpgds	Fabp5	H2-Oa	Ngp	Mrc1
Mxd1	Plcb1	Ear2	Cd72	C1qa	Zfp366	Inhba	Sult1a1
Taldo1	Ahnak	Grk3	Cdk18	Syngr1	Gpr68	Orm1	Pf4
Il1b	F13a1	Dusp16	Col14a1	Mmp12	H2-DMb2	Serpinb1a	Fxyd2
Gsr	Vcan	Cyth3	Arhgap22	Rps20	Ccnd1	Cd177	Fcrls
Il1f9	Ms4a6c	Nr4a1	C3ar1	Fth1	Kit	Adpgk	Chp2
Sorl1	Ms4a8a	Fabp4	Pcp4l1	Rpl39	P2ry10	Olfml2b	Ccl24
Stk17b	Ifi209	Myo1g	Itga9	Spp1	Tbc1d4	Tst	Slco2b1
Fgl2	Itgb7	Smpdl3b	Adcy3	Ppia	Cd209a	1700020L24Rik	Stab1
H2-Q10	Vim	Smc6	Blnk	Lgals3	Klrb1b	Slco4c1	Maf
S100a8	Ms4a6b	Nxpe4	Zmynd15	Rps24	Avpi1	1700047M11Rik	Pmp22
S100a9	Slfn5	Itga4	Gatm	Lgals1	Ece1	Ppp1r42	Dab2

My.08	My.09	My.10	My.11
Nlrp3^{hi} M1 MF	**Mox MF**	**Fn1^{hi} MF**	**pDC**
Ptgs2	Nqo1	Tgfb2	Gm21762
Acod1	Il4i1	Gata6	Havcr1
Il1r2	Cd300e	Ltbp1	Klk1
Ptgs2os2	Abcc1	Gbp2b	Pacsin1
Csrnp1	Mmp14	Ptgis	Cacna1e
Cxcl2	Bcl2a1d	Mlxipl	Cox6a2
Trem1	Zc3h12c	Efnb2	Tbxa2r
Lmnb1	Txnrd1	Gm10369	Atp2a1

Hcar2	Cd274	Ackr3	Klk1b27
Slc7a11	Gm20658	Fam171a1	Sh3bgr
Srgn	Mllt6	Gm16104	Atp1b1
Il1b	Tnip1	Calml4	Gm14964
Ets2	Cyth3	Jam2	Ccdc162
Csf1	Adrb1	Fam20a	Pnck
Clec4d	Acp2	Platr26	Xkrx
Pim1	Ly9	Prg4	Cdh5
Ier3	Clec4n	Fabp7	Cd300c
Nfkbia	Pparg	Garnl3	Slc22a12
Ccrl2	Bcl2	Bcam	Chdh
Clec4e	Gstm1	Gprc5b	Hs3st1

Major Resources Table
Animals (in vivo studies)

Species	Vendor or Source	Background Strain	Sex	Persistent ID / URL
Mouse, *Ldlr*$^{-/-}$	Jackson	C57BL/6J	Female	www.jax.org
Mouse, *Apoe*$^{-/-}$	Jackson	C57BL/6J	Female	www.jax.org
Mouse, wildtype C57BL/6J	Jackson	C57BL/6J	Female	www.jax.org

Antibodies

Target antigen	Vendor or Source	Catalog #	Working concentration	Lot # (preferred but not required)	Persistent ID / URL
Mouse					
MOMA-2	Bio-Rad (formerly AbD Serotec)	MCA519G	1:1000	N/A	www.bio-rad-antibodies.com
α-Rat	Vector	BA-4001	1:200	N/A	www.vectorlabs.com
CD4 – V500	BD Biosciences	560782	1:1000	N/A	www.bdbiosciences.com
CD8a – AF700	Biolegend	100730	1:500	N/A	www.biolegend.com
CD62L - APC	eBioscience	17-0621-82	1:1000	N/A	www.thermofisher.com/ebioscience
CD44 – PE-Cy7	Biolegend	103030	1:1000	N/A	www.biolegend.com
CD19 – BV605	Biolegend	115540	1:500	N/A	www.biolegend.com
CD11b – PE	eBioscience	12-0112-82	1:1000	N/A	www.thermofisher.com/ebioscience
CD11c – FITC	Biolegend	117306	1:800	N/A	www.biolegend.com
Ly6G – PerCP	Biolegend	127654	1:500	N/A	www.biolegend.com
Ly6C – PE-CF594	BD Biosciences	562728	1:800	N/A	www.bdbiosciences.com

CD8a – PE-Texas Red	Invitrogen	MCD0817	1:1000	N/A	www.thermofisher.com/invitrogen
IFNγ – AF488	Biolegend	505813	1:100	N/A	www.biolegend.com
IL-17A – PE	Biolegend	506904	1:100	N/A	www.biolegend.com
IL-4 – PE-Cy7	Biolegend	504118	1:100	N/A	www.biolegend.com
IL-10 – APC	eBioscience	17-7101-82	1:100	N/A	www.thermofisher.com/ebioscience
CD45 – AF700	Biolegend	103128	1:1000	N/A	www.biolegend.com
CD3 – eFluor450	eBioscience	48-0032-82	1:200	N/A	www.thermofisher.com/ebioscience
CD11b – BV605	Biolegend	101257	1:500	N/A	www.biolegend.com
PD-1 – PerCP. Cy5.5	Biolegend	109120	1:400	N/A	www.biolegend.com
Ly6C – APC	eBioscience	17-5932-82	1:500	N/A	www.thermofisher.com/ebioscience
CD45 – AF700	Biolegend	103128	1:1000	N/A	www.biolegend.com
Tox – PE	Miltenyi Biotec	130-120-716	1:400	N/A	www.miltenyibiotec.com
CD11b – PE-Dazzle594	Biolegend	101256	1:1000	N/A	www.biolegend.com
CD11c – APC	eBioscience	17-0114-82	1:500	N/A	www.thermofisher.com/ebioscience
CD21 – BV421	Biolegend	123422	1:400	N/A	www.biolegend.com
CD23 – FITC	Biolegend	101605	1:600	N/A	www.biolegend.com
T-bet – PE-Cy7	eBioscience	25-5825-82	1:1000	N/A	www.thermofisher.com/ebioscience
CD45 – PE	Biolegend	103106	1:500	N/A	www.biolegend.com
CD16/32 (Fc Block)	BD Biosciences	553142	1:250	N/A	www.bdbiosciences.com
Fixable viability dye – eFluor 450	eBioscience	65-0865-18	1:2000	N/A	www.thermofisher.com/ebioscience
Human					
CD45 – PE-Cy7	eBioscience	25-9459-42	1:20	N/A	www.thermofisher.com/ebioscience
CD3 – BV421	Biolegend	317344	1:20	N/A	www.biolegend.com
CD4 – PerCP-Cy5.5	Biolegend	317428	1:20	N/A	www.biolegend.com
CD8 – BV510	Biolegend	344731	1:20	N/A	www.biolegend.com

PD-1 – BV650	Biolegend	329918	1:20	N/A	www.biolegend.com
TOX – PE	Miltenyi	130-120-716	1:80	N/A	www.miltenyibiotec.com
GZMK – APC	Biolegend	370509	1:20	N/A	www.biolegend.com
CD45 – APC	Biolegend	3688512	1:20	N/A	www.biolegend.com
CD19 – FITC	Biolegend	302206	1:20	N/A	www.biolegend.com
CD11b – PE	Beckman & Coulter	IM2581U	1:20	N/A	www.beckman.com
CD11c – eFluor450	eBioscience	48-0116-41	1:20	N/A	www.thermofisher.com/ebioscience
T-bet – PE-Cy7	Invitrogen	25-5825-82	1:40	N/A	www.thermofisher.com/invitrogen
TruStain FcX	Biolegend	422302	1:20	N/A	www.biolegend.com
Fixable viability dye – eFluor 450	eBioscience	65-0865-18	1:2000	N/A	www.thermofisher.com/ebioscience

Data & Code Availability

Description	Source / Repository	Persistent ID / URL
Sequencing data	Available upon request	

Other

Description	Source / Repository	Persistent ID / URL
Trichrome Stain (Masson) Kit	Sigma Aldrich	www.sigmaaldrich.com
Oil Red O	Sigma Aldrich	www.sigmaaldrich.com
Hematoxylin Solution, Mayer's	Sigma Aldrich	www.sigmaaldrich.com
RPMI 1640	Gibco	www.thermofisher.com
Vectastain ABC kit (PK-4000)	Vector	www.vectorlabs.com
ImmPact NovaRed kit	Vector	www.vectorlabs.com
Collagenase I	Sigma Aldrich	www.sigmaaldrich.com
Collagenase XI	Sigma Aldrich	www.sigmaaldrich.com
Hyaluronidase	Sigma Aldrich	www.sigmaaldrich.com
DNAse I	Sigma Aldrich	www.sigmaaldrich.com
Fetal Bovine Serum	Greiner Bio-One	www.gbo.com
Phorbol 12-myristate 13-acetate	Sigma Aldrich	www.sigmaaldrich.com
Ionomycin	Sigma Aldrich	www.sigmaaldrich.com
Brefeldin A	Biolegend	www.biolegend.com
RPMI 1640	Gibco	www.thermofisher.com
Collagenase IV	ThermoFisher Scientific	www.thermofisher.com
DNAse I	Sigma Aldrich	www.sigmaaldrich.com
Albumin from Human Serum	Sigma Aldrich	www.sigmaaldrich.com
Ficoll Paque Premium™	Sigma Aldrich	www.sigmaaldrich.com